

## THE COLOR-MAGNITUDE RELATION IN CL 1358+62 AT $Z = 0.33$ : EVIDENCE FOR SIGNIFICANT EVOLUTION IN THE S0 POPULATION

PIETER G. VAN DOKKUM, MARIJN FRANX

Kapteyn Astronomical Institute, P.O. Box 800, NL-9700 AV, Groningen, The Netherlands

DANIEL D. KELSON, GARTH D. ILLINGWORTH

University of California Observatories / Lick Observatory, Board of Studies in Astronomy and Astrophysics, University of California, Santa Cruz, CA 95064

DAVID FISHER

Kapteyn Astronomical Institute, P.O. Box 800, NL-9700 AV, Groningen, The Netherlands

AND

DANIEL FABRICANT

Harvard-Smithsonian Center for Astrophysics, 60 Garden Street, Cambridge, MA 02318

*Accepted for publication in the Astrophysical Journal*

### ABSTRACT

We use a large, multi-color mosaic of HST WFPC2 images to measure the colors and morphologies of 194 spectroscopically confirmed members of the rich galaxy cluster CL 1358+62 at  $z = 0.33$ . We study the color-magnitude (CM) relation as a function of radius in the cluster, to a limit of 4.6 arcmin from the center, equivalent to  $1.6 h_{50}^{-1}$  Mpc.

The intrinsic scatter in the restframe  $B-V$  CM relation of the elliptical galaxies is very small:  $\sim 0.022$  magnitudes. The CM relation of the ellipticals does not depend significantly on the distance from the cluster center. In contrast, the CM relation for the S0 galaxies does depend on radius: the S0s in the core follow a CM relation similar to the ellipticals, but at large radii ( $R > 0.7 h_{50}^{-1}$  Mpc) the S0s are systematically bluer and the scatter in the CM relation approximately doubles to  $\sim 0.043$  magnitudes. The blueing of the S0s at large radii is significant at the 95 % confidence level.

These results imply that the S0 galaxies in the outer parts of the cluster have formed stars more recently than the S0s in the inner parts. A likely explanation is that clusters at  $z = 0.33$  continue to accrete galaxies and groups from the field and that infall extinguishes star formation. The apparent homogeneity of the elliptical galaxy population implies that star formation in recently accreted ellipticals was terminated well before accretion occurred.

We have constructed models to explore the constraints that these observations place on the star formation history of cluster galaxies. The best constrained parameter is the scatter in the luminosity-weighted age  $\Delta\tau_L / \langle\tau_L\rangle$ , which is less than 18 % for the ellipticals and the S0s in the cluster core, and less than 35 % for the S0s in the outer parts of the cluster. The constraints on the most recent period of star formation are model dependent, but we show that star formation in ellipticals likely ceased at  $z = 0.6$  or higher. If we assume that the galaxies have a constant star formation rate up to a randomly distributed truncation time, we find that the S0s in the outer parts of the cluster have experienced star formation until the epoch of observation at  $z = 0.33$ .

We conclude that the population of S0s in clusters is likely to evolve as star forming galaxies are converted into passively evolving galaxies. Assuming a constant accretion rate after  $z = 0.33$ , we estimate  $\sim 15\%$  of the present day early-type galaxy population in rich clusters was accreted between  $z = 0.33$  and  $z = 0$ . The ellipticals (and the brightest S0s) are probably a more stable population, at least since  $z = 0.6$ .

*Subject headings:* galaxies: evolution, galaxies: elliptical and lenticular, cD, galaxies: structure of, galaxies: clusters: individual (CL 1358+62)

### 1. INTRODUCTION

Early-type galaxies in nearby rich clusters form a homogeneous population. The elliptical and S0 galaxies in clusters such as Coma follow a tight color-magnitude (CM) relation (Bower, Lucey, & Ellis 1992b),  $Mg_2-\sigma$  relation (Guzman et al. 1992), and Fundamental Plane (e.g., Jørgensen, Franx, & Kjørgaard 1993). The low scatter in these relations implies that the spread in the metallicities and ages of the galaxies is small at a given mass or luminosity.

The homogeneity of the early-type galaxies constrains models for the formation and evolution of these galaxies (e.g., Sandage & Visvanathan 1978, Faber et al. 1987, Bower et al. 1992b). In particular, the small intrinsic scatter in the CM relations of Coma and Virgo implies that the early-type galaxies in these clusters either formed at high redshift, or that their for-

mation was synchronized (Bower et al. 1992b).

If the intrinsic scatter is due to age differences between the galaxies, one expects the scatter to be higher at larger look-back times. Hence, the scatter in the CM relation is expected to increase with redshift. Ellis et al. (1997) studied the CM relation in three clusters at  $z \sim 0.55$  using Hubble Space Telescope (HST) data. Surprisingly, Ellis et al. (1997) found that the CM relation of the ellipticals and S0s is still very tight at  $z = 0.55$ . This led these authors to conclude that the star formation in early-type galaxies likely ceased at much higher redshifts. A similar conclusion was reached by Andreon, Davoust, & Heim (1997), who found a tight CM relation of the early-type galaxies in Abell 851 at  $z = 0.4$ . These results were further strengthened by Stanford, Eisenhardt, & Dickinson (1997), who found that the scatter in the CM relation of early-type galaxies in rich

clusters is nearly constant with redshift to  $z \sim 0.9$ . Similarly, studies of the Fundamental Plane relation in clusters to  $z \sim 0.6$  show that the scatter in the relation is not very different from that in local clusters (van Dokkum & Franx 1996; Kelson et al. 1997; Bender et al. 1997), indicating that the population of early-type galaxies has been stable and homogeneous over a significant fraction of the age of the universe.

The result of Ellis et al. (1997) is surprising, because it seems difficult to reconcile with the strong evolution of the cluster population implied by the Butcher-Oemler effect. The enhanced fraction of blue galaxies in intermediate redshift clusters as observed by Butcher & Oemler (1978, 1984) is often interpreted as the result of the transformation of blue field galaxies to red cluster galaxies (e.g., Butcher & Oemler 1984, Abraham et al. 1996b). A key question is whether the end products of this transformation are early-types (e.g., Dressler et al. 1997), or whether the Butcher-Oemler effect can be largely explained by blue spirals turning red (Butcher & Oemler 1984). Many blue galaxies in intermediate redshift clusters have the characteristics of normal (field) spirals (e.g., Couch & Sharples 1987, Andreon et al. 1997). However, some have a starburst or a post starburst spectrum (Dressler & Gunn 1983; Couch & Sharples 1987), and it seems natural to link these post starburst galaxies to today's early-type galaxies. If a population of recently transformed early-types exists, they are expected to be bluer than the pre-existing early-types, and to increase the scatter in the CM relation. Apparently, such galaxies are not in the samples studied by Ellis et al. (1997) and Stanford et al. (1997). On the other hand, the strong evolution with redshift of the morphology-density relation claimed by Dressler et al. (1997) is in qualitative agreement with the continuous transformation of spirals to S0s.

The studies of Ellis et al. (1997) and Stanford et al. (1997) suffer from two limitations: membership information is sparse, and the field sizes are small. The membership information is important because it is crucial to measure the full distribution of galaxies in the color-magnitude plane, and the blue side of the CM relation is heavily contaminated by field galaxies. Usually, a correction is applied by subtracting the expected number of field galaxies based on number counts. Since the number counts can vary in a small field, it is obviously preferable to have direct spectroscopic membership information.

A large angular coverage is of particular importance, since there is good evidence that the blue galaxies are more abundant at larger distances from the cluster center (e.g., Butcher & Oemler 1984, Pickles & van der Kruit 1991, Abraham et al. 1996b). An environmental dependence is also indicated by the evidence for young populations in early-type galaxies in the field (e.g., Larson, Tinsley, & Caldwell 1980, Bothun & Gregg 1990). If there are (mildly) blue early-type galaxies in intermediate redshift clusters, it seems likely that they reside in the transition region between the cluster and the field.

In the present study, we extend the study of the CM relation to larger radii, using a large  $8' \times 8'$  HST mosaic of the cluster CL 1358+62 at  $z = 0.33$ . We determine morphologies, colors, and magnitudes for 194 spectroscopically confirmed cluster members within the HST mosaic. The color-magnitude relation in intermediate redshift clusters has been studied extensively (e.g., Aragon-Salamanca et al. 1993, Rakos & Schombert 1995, Abraham et al. 1996b, Ellis et al. 1997, Stanford et al. 1997), but never before with high resolution, large format images. The aims of this study are to constrain the star formation

histories of the galaxies, and to establish whether the histories depend on morphology or environment. In particular, we test whether star formation in the ellipticals and S0 galaxies in the outer parts of the cluster has persisted to more recent epochs than star formation in early-type galaxies in the cluster core.

## 2. DATA

### 2.1. Sample Selection

The present sample is based on a large spectroscopic survey of the cluster. The spectra were obtained with multislit masks at the Multiple Mirror Telescope and the William Herschel Telescope. The sample selection and the reduction and analysis of the spectroscopic data are described in detail in Fabricant, McClintock, & Bautz (1991), and Fisher et al. (1997). Here, we briefly summarize the sample selection.

The spectroscopic sample was selected on the basis of  $R$  magnitude. Twenty multislit aperture masks were exposed within a  $\sim 10' \times 11'$  field centered on the brightest cluster galaxy in CL 1358+62, and redshifts for 387 galaxies were determined. The sample of galaxies with redshifts is  $> 80\%$  complete to  $R = 21$ , or  $F814W \sim 20.2$ , dropping steeply to  $\sim 20\%$  at  $R = 22$  ( $F814W \sim 21.2$ ). The completeness within the  $8' \times 8'$  HST WFPC2 field (see below) is somewhat higher:  $> 90\%$  to  $R = 21$ , and  $\sim 30\%$  at  $R = 22$ . This incompleteness is caused by the limited number of galaxies that was observed, and not by the inability to measure the redshifts of observed galaxies. The "success rate" of measuring the redshift is 100% to  $R = 21.1$ . The success rate drops to 70% at  $R = 22.3$  ( $F814W \sim 21.5$ ), and 50% at  $R = 23$ . The success rate does not depend strongly on color, for  $R < 23.5$  (Fisher et al. 1997).

We refer the reader to Fisher et al. (1997) for a discussion of cluster membership and substructure in the cluster. Following Fisher et al., we include as cluster members all galaxies in the interval  $0.31461 < z < 0.34201$ . The subsample used for this paper consists of all 194 confirmed cluster members in the  $8' \times 8'$  HST WFPC2 field (see below). For the analysis in Sect. 3, we furthermore impose a magnitude limit of  $F814W = 21.5$ , reducing the sample to 188 galaxies.

### 2.2. Imaging

WFPC2 images from twelve HST pointings were combined to give an  $\sim 8' \times 8'$  field centered on the brightest cluster galaxy (BCG) in CL 1358+62. The cluster was observed with the  $F606W$  and  $F814W$  filters (close to rest frame  $B$  and  $V$ ), on February 15, 1996. Exposure times were 3600s in each filter, for each pointing. Figure 1 [Plate 1] shows the field layout.

#### 2.2.1. Reduction

The pipeline reduction was performed at the Space Telescope Science Institute (STScI). No recalibration was done, and we verified that the most recent calibration files had been used in the pipeline processing. The crucial step in the data reduction was the sky subtraction. The cluster was observed in the Continuous Viewing Zone (CVZ) of HST. The sky background is fairly high in most exposures, due to reflected Earth light. The Earth light reflects off the Optical Telescope Assembly (OTA) and scatters throughout the WFPC2 field. In most exposures, dark diagonal bands are present; these appear when the OTA vanes pass into the shadow of the WFPC2 camera relay spiders (see Biretta, Ritchie, & Rudloff 1995).

Three identical 1200 s exposures were obtained in each filter. The exposures were timed to minimize the scattered light in one of the three exposures. For the majority of exposures, we modelled the background in two steps. First, the image with the lowest background was subtracted from the two other images. Second, the residual images (containing the background structure + noise) were fitted with high order 2D polynomials. These fits were then subtracted from the high background images. Finally, we checked the results by eye and iterated to minimize the residuals of the cross patterns. In all *F606W* exposures this method worked well. However, in four of the twelve *F814W* pointings the background structure was present in all three exposures. For these pointings, the cross pattern in the lowest background image was carefully fitted and subtracted before subtracting this image from the higher background images.

In 10 of the 72 exposures bright linear features are present, due to the passage of bright objects through the field of view during the exposures (Biretta et al. 1995). The areas affected by these features were masked before the three exposures of each field were combined. When both a high background and a bright streak are present, the bright streak was masked before modeling the background.

The individual exposures were combined with the CRREJECT task, incorporated in the IRAF STSDAS reduction package. The output cosmic ray mask files were visually checked to verify that only cosmic rays were removed. Hot pixels were corrected by creating a “dark” frame from the exposures themselves; the twelve pointings were median filtered to identify the locations of hot pixels. Bad pixels and bad columns were removed by interpolation.

The full field is shown in Fig. 1 [Plate 1]. The total area of the image is 49 arcmin<sup>2</sup>. The galaxy density decreases with distance from the BCG, allowing us to study the dependence of the properties of the cluster galaxies on local galaxy density. Fig. 2 [Plate 2] is a color image of the central part of the cluster. Clearly, most of the cluster galaxies have very similar colors, but our spectroscopy shows that many of the blue galaxies are also cluster members (Fisher et al. 1997).

### 2.2.2. Zeropoints

The *F606W* and *F814W* HST WFPC2 filters are close to the rest frame *B* and *V* bands for an object with  $z = 0.33$ . As noted by many authors, standard *K*-corrections may introduce large errors, due to the effects of spectral evolution and intrinsic scatter in galaxy colors. Therefore, we followed the procedure described in van Dokkum & Franx (1996), and derived direct transformations from the HST filters to the redshifted *V* band, denoted with  $V_z$ , and  $(B-V)_z$  colors:

$$V_z = F814W + 0.20(F606W - F814W) + 0.65 \quad (1)$$

$$(B-V)_z = 0.82(F606W - F814W) - 0.13 \quad (2)$$

For the early-type galaxies in CL 1358+62,  $V_z \sim F814W + 0.9$ . The zero points of the *F814W* and *F606W* filters are based on the Vega spectrum, and taken from Table 41.1 in the HST Data Handbook (Leitherer 1995). Using spectral energy distributions from Pence (1976), we find the transformations are independent of galaxy type to  $\sim 0.01$  magnitudes, for early-types and early-type spirals.

## 2.3. Morphologies and Photometry

### 2.3.1. Visual Classification

We have extracted  $6''4 \times 6''4$  images of all 194 galaxies from the WFPC2 frames. Greyscale representations of these images are presented in Fig. 3 [Plate 3]. Four of us (PvD, MF, DK, and GDI) morphologically classified the galaxies. Our classification scheme is identical to that used by Dressler (1980) for galaxies in nearby clusters. Five morphological types are distinguished: E, S0, S, Irregular, and unclassified. These morphological types were assigned on the basis of two qualifiers: early-type/late-type/irregular, and disk/no disk/irregular. The division between late-type and early-type is determined by the presence of spiral arms and the smoothness of the image. The disk qualifier is based on the presence of a disk. Because faint, face-on disks in S0 galaxies are very difficult to detect, early-type galaxies that were classified as diskless may contain disks at low inclinations (see, e.g., Rix & White 1990, Jørgensen & Franx 1994).

If at least three out of four authors agreed on the value of the qualifier the value was set to the median of the values of the four authors. If there was no such agreement, the type qualifier and / or disk qualifier were set to “uncertain”. Our classifications fit directly into Dressler’s (1980) scheme. Ellipticals are early-type galaxies without a disk, S0s are early-type galaxies with a disk, and spirals are late-type galaxies with a disk. Galaxies with type and/or disk qualifier “irregular” are classified as irregulars. The classifications are listed in Table 1, and labeled in Fig. 3 [Plate 3]. Color representations of several examples of galaxies of different morphologies are shown in Fig. 4 [Plate 4].

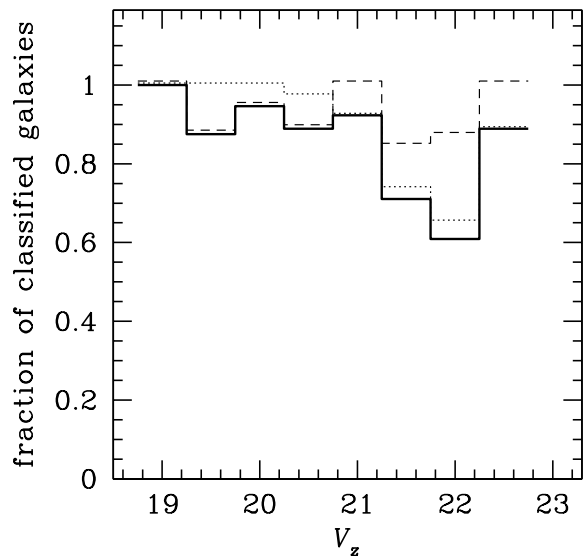


Fig. 5.— The agreement between visual classifications of different authors. The histograms show the fraction of galaxies within a magnitude bin that were given identical classifications by at least three out of four authors. The agreement on the type qualifier is indicated by the dashed line, and the agreement on the disk qualifier by the dotted line. The drawn line indicates the agreement on the type qualifier and the disk qualifier simultaneously. The magnitude bins are 0.5 magnitudes wide. Adjacent points are independent.

The reliability of visual classifications has been discussed ex-

tensively (e.g., Abraham et al. 1996a, Smail et al. 1997). It appears that the robustness of the classification of HST images of galaxies at  $z \lesssim 0.5$  is not very different from that of the classification of galaxies in nearby clusters observed from the ground; even at low redshift it is difficult to distinguish between adjacent Hubble types. The robustness of the classification can be assessed by comparing the classifications of different authors. Figure 5 illustrates the consistency of the classifications. Three of the four authors agree on  $> 85\%$  of the galaxies to  $V_z = 21$ . The improvement in the consistency of the classifications at magnitudes fainter than  $V_z = 22$  is probably real. The galaxy sample is dominated by irregular galaxies below this magnitude, and these galaxies are more easily distinguished from the other types than, e.g., ellipticals from S0s.

Some of the galaxies in the sample have faint, smooth spiral structure (e.g., galaxy 328). In the adopted classification scheme, these galaxies could either be classified as spirals (on the basis of the spiral features), or S0s (on the basis of the absence of star formation regions and dust). It is not clear how these galaxies fit into the Hubble sequence. We will discuss the properties of these galaxies in more detail in future papers on the morphology-density relation, and the “E+A” galaxies in CL 1358+62. We note here that four of these ambiguous galaxies were classified as S0s, the remainder as spirals.

We compared the limiting magnitude of our classifications to the limits adopted by Smail et al. (1997) and Ellis et al. (1997). Smail et al. classify galaxies to a limit (in signal-to-noise)  $\sim 1$  magnitudes fainter than in our study, and Ellis et al. to a limit  $\sim 0.5$  magnitudes fainter.

### 2.3.2. Quantitative Classification from Structural Parameters

The visual classifications are by their nature not very quantitative, nor can we assess systematic errors. Because the vast majority of cluster galaxies in the present sample are early-type galaxies, it is desirable to have a quantitative indicator of the bulge-to-disk ratios of these galaxies, to have an alternative way to discriminate between bulge dominated and disk dominated galaxies. As noted by Saglia et al. (1997), the Sérsic (1968)  $n$  parameter provides a rough measure of the bulge-to-disk ratio. The value of  $n$  that gives the lowest  $\chi^2$  in a fit of the galaxy profile to an  $r^{1/n}$  law depends on the relative contributions of the bulge and the disk. If the disk dominates,  $n$  will be close to 1 (i.e. an exponential profile), if the bulge dominates,  $n$  will be close to 4 (i.e. the de Vaucouleurs  $r^{1/4}$  law).

All images of the cluster galaxies were fitted with two-dimensional  $r^{1/n}$ -law models (Sérsic 1968), with  $1 \leq n \leq 4$ , which were convolved with the HST Point Spread Function (PSF). The PSFs were generated with Tiny Tim 4.0b (Krist 1995). For each galaxy, a separate PSF was used, appropriate to the galaxy position on the WF chip. The fitting method uses the full 2D information rather than an azimuthally averaged light profile. The fitting program determines the position, ellipticity, position angle, effective radius  $r_e$ , and the surface brightness at the effective radius  $\mu_e$ . The method is described for the  $n = 4$  case (the de Vaucouleur  $r^{1/4}$ -law) in van Dokkum & Franx (1996). Models with  $n = 1, 2, 3, 4$  were fitted to the galaxy images. The  $\chi^2$  values of the four fits were compared to choose the ‘best fitting profile type’ for each galaxy.

We have performed simulations to test how well the  $n$  parameter correlates with bulge-to-disk ratio. Artificial galaxies were created with varying bulge-to-disk ratios, inclinations, and effective radii of the bulges and the disks. The effective radii

of the disks span a range from half the effective radius of the bulge to twice the effective radius of the bulge. In the simulations, the surface brightness profiles of the bulges follow  $r^{1/4}$  laws, and the surface brightness profiles of the disks are exponential. The artificial galaxies were convolved with Tiny Tim PSFs, before determining the  $n$  parameter. We used the same procedure to determine the best fitting profile type  $n$  as for the cluster galaxies.

The simulations show that the  $n$  parameter does indeed correlate with bulge-to-disk ratio, but that it is also somewhat dependent on the effective radius of the disk relative to the bulge: large, faint disks relative to the bulge give rise to higher  $n$  values than small, bright disks. Bulge fractions  $\leq 20\%$  give rise to  $n \leq 2$  in 90% of the cases, and bulge fractions  $\geq 70\%$  always give rise to  $n \geq 3$  in our simulations.

In reality, galaxy profiles cannot always be described by the combination of a de Vaucouleurs bulge and an exponential disk. As an example, galaxy 86 is one of 2 galaxies that are best fitted by an exponential profile ( $n = 1$ ), but are visually classified as elliptical. A closer examination of its surface brightness profile reveals that it is best fitted by a combination of two exponentials. Also, bars and other non-axisymmetric features complicate the interpretation of the  $n$  parameter.

In summary, the  $n$  parameter is a rough measure of the bulge-to-disk ratio, but one should be cautious in drawing conclusions for individual galaxies on the basis of the  $n$  parameter. We stress that the  $n$  parameter is not intended as a refinement of the visual classifications, but as an independent and quantitative measure of the morphology. We will express our results in the context of both the visual classifications, and the best fitting profile type.

### 2.3.3. Colors and Magnitudes

The colors were measured from aperture photometry using the PHOT task in IRAF. For each galaxy, the radius of the aperture  $r_c$  was set equal to the effective radius,  $r_e$ , as determined from the fit to an  $r^{1/4}$ -law. The advantage of using the effective radius rather than a larger aperture is that sky subtraction errors are small. Furthermore, this procedure minimizes the effects of color gradients.

For many galaxies, the effective radii are  $\lesssim 0''.5$ . Within such small radii, the galaxy profiles are significantly affected by the Point Spread Function (PSF). The shape of the HST PSF depends on the passband, and the measured colors within an effective radius are affected by the differences between the  $F606W$  and  $F814W$  PSFs. We determined the importance of this effect by constructing a model galaxy with an effective radius of  $0''.3$ , and convolving it with  $F606W$  and  $F814W$  PSFs generated by Tiny Tim. The measured color within  $r_c$  turned out to be 0.016 magnitudes bluer than the true color. After deconvolution of the model galaxy, the true color could be obtained within 0.001 magnitudes. We tested whether the Tiny Tim PSF is a reasonable approximation of the true PSF by constructing a model galaxy using the  $F606W$  and  $F814W$  images of a star in the field, and deconvolving it using a Tiny Tim PSF. Again, the true color could be obtained within 0.001 magnitudes after deconvolution.

To correct for the effects of the PSF, we deconvolved all images before measuring the colors. For the deconvolutions the CLEAN algorithm (Högbom 1974) was used, which ensures flux conservation. For each galaxy a PSF was created with Tiny Tim, appropriate for the position of the galaxy on the chip. The deconvolution does not influence the scatter in the CM relation

significantly. However, the deconvolution has a small, but systematic, effect on the slope of the CM relation.

We performed extensive tests to establish how our conclusions depend on the choice of aperture. We explored the effect of apertures with radii  $r_c/2$ ,  $2r_c$ , and  $3r_c$ , as well as apertures with a fixed angular radius ( $0''.2$ ,  $0''.6$ ,  $1''.0$ , and  $1''.5$ ). The systematic trends discussed in Sect. 3.2 also apply for all these apertures. However, the colors of individual galaxies may depend substantially on the aperture size because some galaxies have significant color gradients. We will return to this issue later.

“Total” magnitudes were measured through  $1''.5$  radius apertures. The error in the total magnitude contributes to the scatter in the CM relation. This can be estimated at  $|\alpha|\delta V$ , where  $\alpha$  is the slope of the CM relation and  $\delta V$  is the error in the magnitude. Since  $|\alpha| \sim 0.018$  (cf. Sect. 3.1) this contribution to the scatter in the CM relation is negligible, for  $\delta V < 1$  magnitude. The colors and magnitudes of all 194 galaxies in the sample are listed in Table 1.

### 2.3.4. Photometric Accuracy

It is difficult to calibrate HST WFPC2 observations to higher absolute accuracy than 5% (see, e.g., Holtzman et al. 1995, Whitmore 1997). One of the main uncertainties is the charge transfer efficiency (CTE) which leads to efficiency variations of a few percent over individual WFPC2 chips (Whitmore 1997). Fortunately, all uncertainties that are effectively efficiency variations over the WFPC2 field (such as the CTE problem) cancel out when determining colors, provided the effect is not very wavelength dependent. Therefore, in principle, color differences between galaxies can be measured to very high accuracy despite limitations in the absolute calibration.

The signal to noise (S/N) ratio in the HST observations of the spectroscopically confirmed cluster members is very high; the formal errors in the colors measured within  $r_c$  are  $\lesssim 0.005$  magnitudes for all galaxies. However, other systematic sources of error remain, e.g., the flatfielding, the sky subtraction, and uncertainties in the PSF.

The HST pointings were chosen to allow an overlap of  $\sim 5''$  between adjacent observations. Therefore, a number of objects in the CL 1358+62 field were observed twice. These repeated observations allow us to directly assess the errors in the photometry. We found 23 objects that were well exposed in two pointings; 15 of these are spectroscopically confirmed cluster members. The galaxy colors were measured within  $0''.7$  radius apertures, which is the median  $r_c$  of the 194 cluster members.

The  $1\sigma$  spread in the differences between the two color measurements of the 23 objects is 0.015 magnitudes, implying an uncertainty for a single observation of  $0.015/\sqrt{2} = 0.011$  magnitudes. The 23 objects span a similar range in magnitude as the sample of 194 cluster members, and have a median magnitude of  $V_z = 21$ . We divided the sample into two bins to determine whether the measurement uncertainty depends on the magnitude. For galaxies with  $V_z < 21$  the uncertainty is 0.009. For galaxies with  $V_z \geq 21$  the uncertainty rises to 0.017 magnitude.

We noticed that the differences between the two observations were often close to  $-0.010$  or  $+0.010$ . This is almost certainly due to systematic differences between the WFPC2 chips: after adding 0.010 to the  $F606W$  zeropoint of chip 3, the measurement uncertainty for galaxies in the bright half of the sample was reduced to 0.002 magnitudes.

The errors in the sky subtraction and the flat fielding are probably largest near the edges of the chips. In addition, the shape of the PSF has a strong positional dependence near the chip edges. Therefore, the color measurement errors for galaxies near the centers of the chips are likely to be smaller than the preceding estimates. The measured scatter in the CM relation of the ellipticals and S0s ranges from 0.021 to 0.043 (cf. Sect. 3), which is significantly larger than the measurement error (0.011). Therefore, the contribution of measurement errors to the measured scatter in the CM relation is generally negligible. However, for consistency, we computed the intrinsic scatter in the CM relation by removing an uncertainty of 0.011 magnitudes in quadrature from the measured scatter.

## 3. THE COLOR-MAGNITUDE RELATION

### 3.1. The Color-Magnitude Relation for Different Morphological Types

The CM relations of cluster members of different morphological types are presented in Figure 6(a-d). The figure shows that the CM relation depends strongly on morphological type. Only the ellipticals and S0s show a well defined relation, whereas the spirals and the irregulars show a large scatter in the color. Few ellipticals are significant outliers from the “ridge line” of this relation, but the fraction of outliers is higher for the S0s. The distribution about the ridge line appears to be tighter for the ellipticals than for the S0s.

We quantified these effects as follows. First, we determined the CM relation for the ellipticals with a least squares fit, excluding the two bluest galaxies. The form of this fit is

$$(B-V)_z = (0.866 \pm 0.004) - (0.018 \pm 0.005)(V_z - 20.7). \quad (3)$$

and it is shown in all upper panels of Fig. 6. For each galaxy we determined the residual color relative to the fiducial CM relation of the ellipticals:  $\Delta(B-V)_z \equiv (B-V)_z + 0.018V_z - 1.240$ . From the distributions of  $\Delta(B-V)_z$  for the different morphological types we determined the offset  $C$  relative to the CM relation of the ellipticals, and the scatter  $\sigma$ . Histograms of the distributions of  $\Delta(B-V)_z$  are shown in Fig. 6(e-h).

The offset and the scatter were calculated using the biweight estimators for the location and the scale of a distribution. This estimator was also used by Stanford et al. (1997). The biweight estimator gives higher weight to points that are closer to the center of the distribution (see Beers, Flynn, & Gebhardt 1990). Therefore, the biweight estimator is insensitive to outliers. For a Gaussian distribution the biweight scale estimator reduces to the conventional rms. The values that we obtain are characteristic of the scatter of the points close to the ridge line, and are insensitive to the blue outliers.

Bower et al. (1992b) and Ellis et al. (1997) use the normalized median absolute deviation (MAD) as a scatter estimator. The biweight estimator is more robust than the MAD estimator (Beers et al. 1990). We checked if our results are sensitive to the choice of estimator by computing the median and the normalized MAD for the distributions, and comparing the results to the biweight estimators. In the present study, the median and the normalized MAD give values very similar to those obtained with the biweight estimators.

Table 1 and Fig. 6 show the offset and the scatter of the CM relation. The error in the scatter was determined from bootstrap resampling. The blue outliers were not excluded from the analysis, although the biweight estimator gives them lower weight.

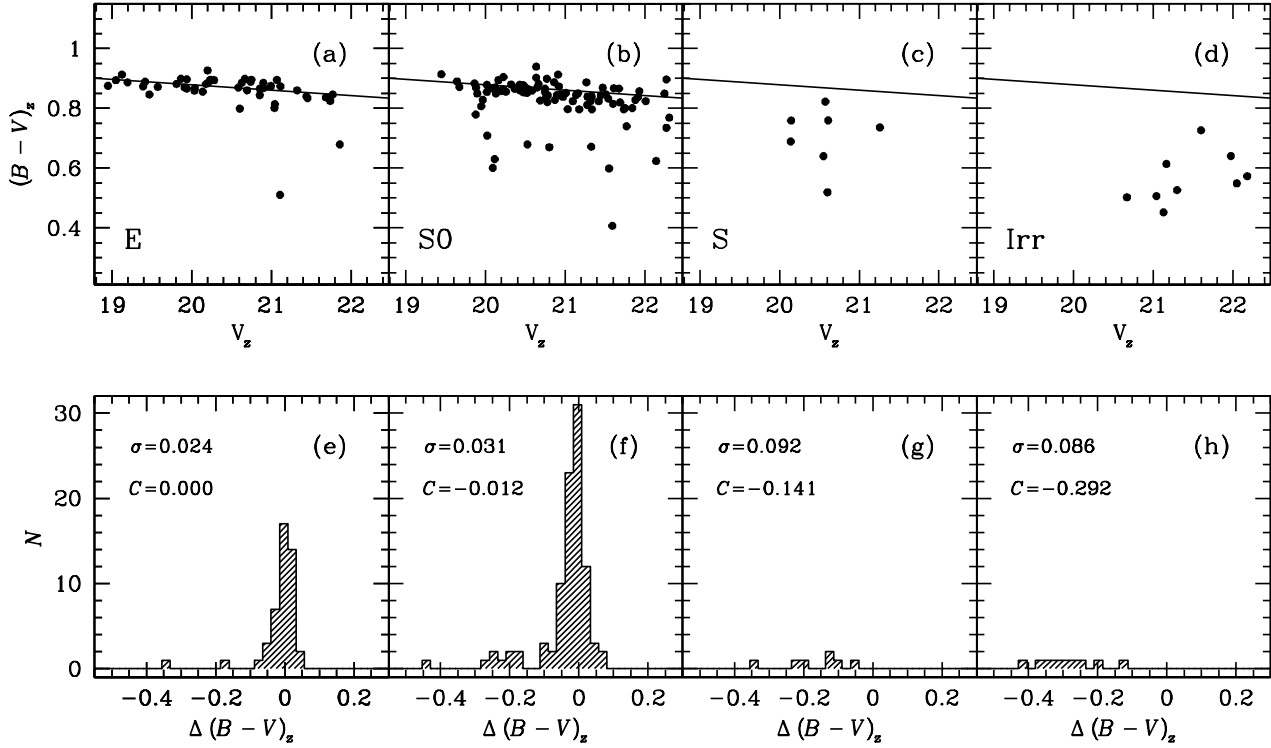


Fig. 6.— The restframe  $B-V$  color-magnitude relation for galaxies of different morphological types (a-d). The line is a least squares fit to the CM relation of the ellipticals, and is repeated in each plot. Panels e-h show the distributions of the colors after subtracting the CM relation of the ellipticals. (see text).

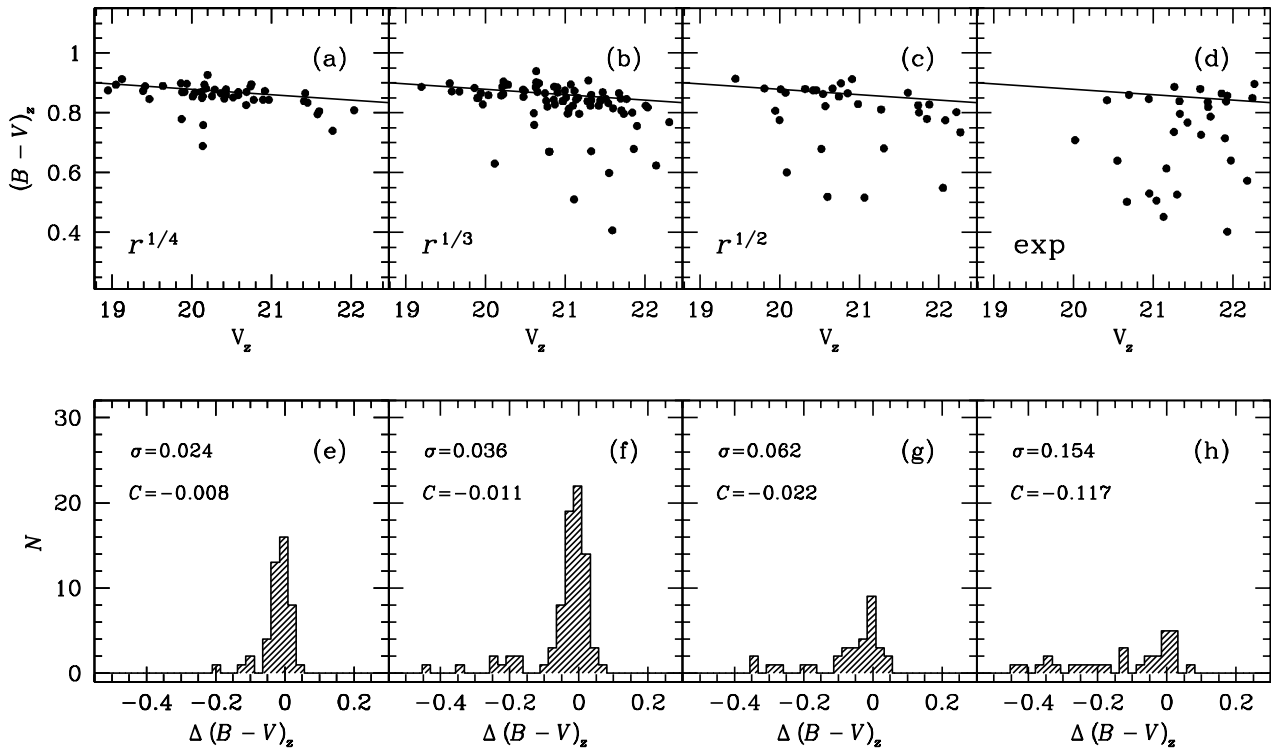


Fig. 7.— The color-magnitude relation for galaxies with different best fitting profile types. Galaxies are systematically bluer and the scatter in the CM relation increases with decreasing  $n$ .

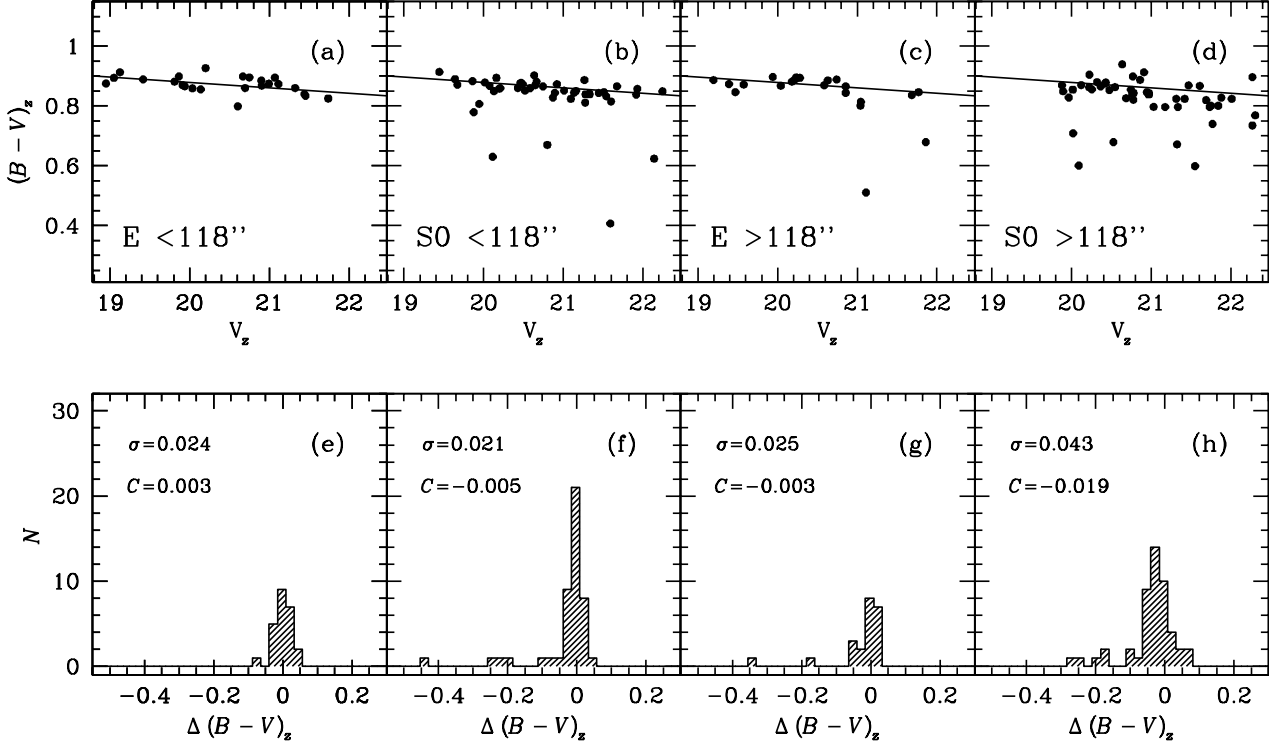


Fig. 8.— Comparison of the color-magnitude relations for ellipticals and S0s in the inner parts and in the outer parts of the cluster. The scatter in the CM relation of the S0s and the Es is very similar inside  $R = 118''$ . Outside  $R = 118''$ , the scatter in the S0 colors is larger than that of the ellipticals by a factor 2.

The visual impression of an increased scatter for the S0 galaxies when compared to ellipticals is confirmed ( $0.031 \pm 0.004$  compared to  $0.024 \pm 0.003$ ). Furthermore, we find that the CM relation of the S0 galaxies is offset to the blue with respect to that of the ellipticals by  $0.012 \pm 0.003$  magnitudes. The significance of the difference in the offsets of the ellipticals and the S0s can be evaluated with the (non-parametric) Mann-Whitney test. The probability that the ellipticals and the S0s are drawn from the same sample is  $< 1\%$ . The difference in the scatter for the ellipticals and S0s is also significant, given the formal errors. We directly determined the significance of the difference between the distributions of the residuals of the CM relations of the ellipticals and the S0s with the Kolmogorov-Smirnov (KS) test. The probability that the distributions were drawn from the same parent sample is 3%.

We tested whether the scatter and offset of the CM relation are functions of the  $n$  value derived from the surface brightness profile fits. In Fig. 7(a-d) the CM relation is shown for different best fitting profile types, ranging from  $r^{1/4}$  ( $n = 4$ ) to exponential ( $n = 1$ ). The distributions of the residuals from the CM relation are shown in Fig. 7(e-h). The offset and the scatter of the CM relation vary systematically with  $n$ , towards a bluer offset and a larger scatter for more disk dominated systems. This trend is exactly the same as the trend with morphology, confirming the distinction between S0s and ellipticals.

This difference in properties between ellipticals and S0s in intermediate redshift clusters has not been seen before. Similar studies of the CM relation with HST have found very low scatter for both ellipticals and S0s (e.g., Ellis et al. 1997). The

main difference with this study is that our large-area imaging extends beyond the cluster core regions covered by previous studies with HST of intermediate redshift clusters. This raises the question whether this effect is related to distance from the cluster center.

### 3.2. Radial Dependence of the Color-Magnitude Relation

We investigated whether the scatter in the CM relation of the ellipticals and S0s depends on  $R$ , the distance from the BCG. As a first test, the galaxy sample was divided into two radial bins. The bin size, 118 arcsec ( $\sim 0.7 h_{50}^{-1}$  Mpc), was chosen such that half of the galaxies classified as early-type are contained in each bin.

Figure 8 shows the CM relation of the ellipticals and S0s inside and outside  $R = 118''$ . The scatter in the CM relation of the ellipticals and the S0s in the inner regions of the cluster is very similar: the observed scatter is  $0.024 \pm 0.004$  for the ellipticals, compared to  $0.021 \pm 0.004$  for the S0s, and the difference in mean color between the ellipticals and the S0s within  $R = 118''$  is not significant.

Although the CM relations of the ellipticals and the S0s appear to be similar in the core of the cluster, they are very different in the outer parts of the cluster. The CM relation of the elliptical galaxies remains essentially unchanged, but the scatter for the S0s increases substantially in the outer parts. The CM relation of the S0s in the outer parts is offset to the blue by 0.019 magnitudes, and the scatter is  $0.043 \pm 0.009$ , almost a factor 2 higher than for the ellipticals in the outer parts, and the ellipticals and S0s in the core. The difference in the mean color

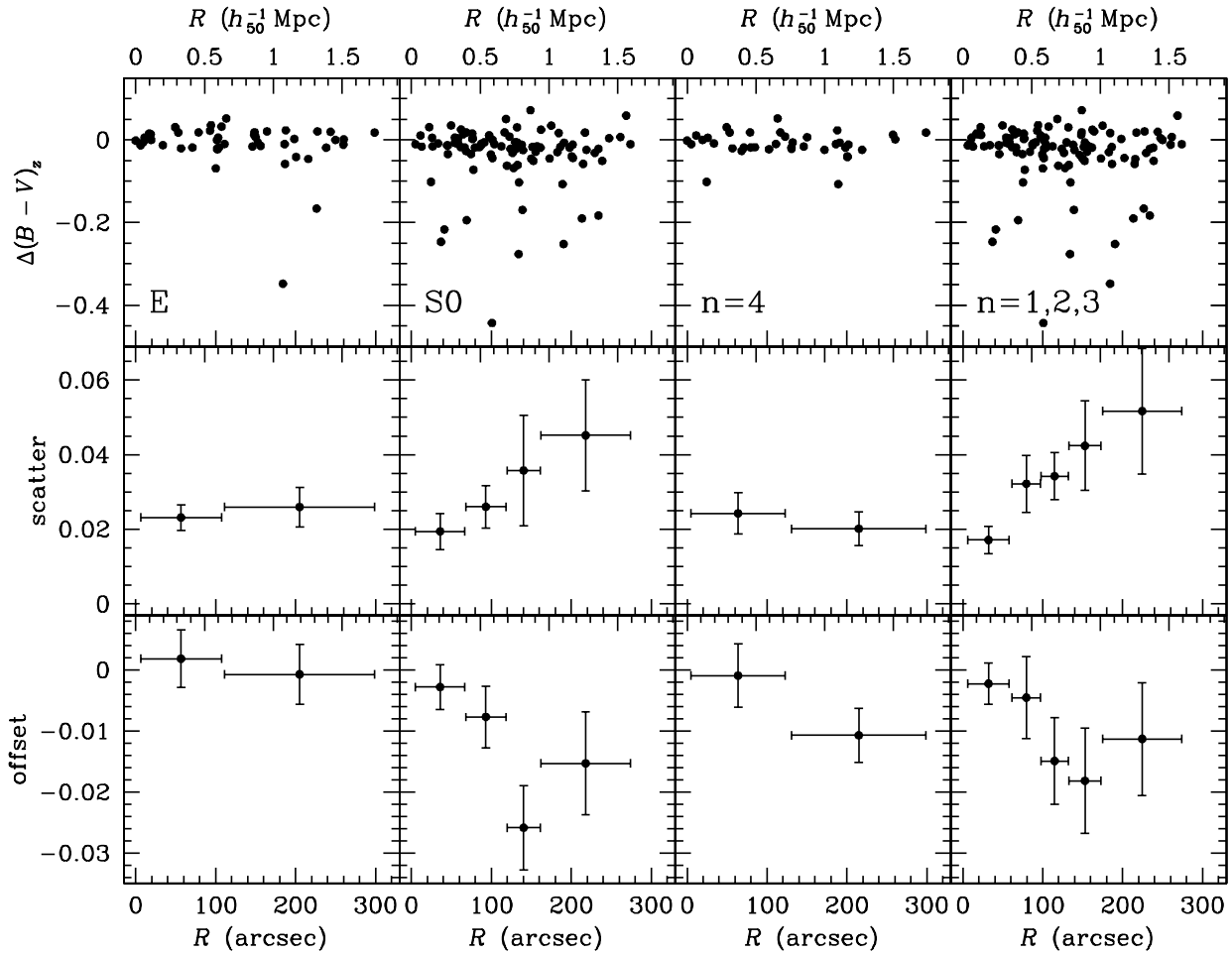


Fig. 9.— The dependence of the residuals from the CM relation on the distance from the BCG, for visually classified ellipticals and S0s, and for early-type galaxies with  $n = 4$  and  $n \leq 3$ , where  $n$  is the value that gives the lowest  $\chi^2$  in a fit to an  $r^{1/n}$  profile. The scatter and offset determined with the biweight estimators are calculated in radial bins, each containing at least 20 galaxies. Adjacent data points are independent. The biweight statistics give low weight to outliers so the scatter is not a direct function of the number of outliers. The scatter in the  $(B-V)_z$  colors of the S0s and the early-types with  $n \leq 3$  increases with  $R$ . These galaxies are also bluer at larger distance from the cluster center. In contrast, the ellipticals and the galaxies best fitted by an  $r^{1/4}$ -law do not show a significant trend with radius, but the number of galaxies is too small to rule out a change with radius in the scatter or mean color of  $\lesssim 0.01$  magnitudes.

between the S0s in the inner parts and the S0s in the outer parts is significant at the 95 % confidence level.

The dependence of the CM relation on the distance to the cluster center can be studied in more detail. In Fig. 9 the residuals of the CM relation are plotted against  $R$ , for visually classified ellipticals and S0s, and for early-type galaxies separated by best fitting profile type. We experimented with the size of the radial bins, and found that the results are robust when there are at least  $\sim 20$  galaxies in each radial bin.

There is a very clear trend of the scatter and mean color for the S0 galaxies, and for the early-type galaxies with  $n \leq 3$ . The trend is much weaker, or absent, for the ellipticals and the early-type galaxies best fitted by a de Vaucouleur  $r^{1/4}$ -law. The scatter in the S0 colors increases from 0.017 at  $R = 40''$  to 0.043 at  $R = 200''$ . The intrinsic scatter increases from 0.013 to 0.042.

The S0s in the outer parts of the cluster are 0.015 magnitudes bluer than the S0s in the inner parts of the cluster. The scatter in the colors of the ellipticals is nearly constant with radius, at 0.024. The ellipticals in the outer parts of the cluster do not appear to be much bluer than the ellipticals in the inner parts. However, the number of elliptical galaxies in the sample is small. We cannot rule out a change in color of  $\sim 0.01$  magnitudes.

These results are confirmed with the objective classification provided by the best fitting profile types; the radial trend for the early-types with  $n \leq 3$  is very similar to the trend for the visually classified S0s. In contrast, there is no evidence for a radial trend in the scatter for the galaxies best fitted by an  $r^{1/4}$ -law, confirming the result for the visually classified ellipticals. The early-types with  $n = 4$  in the outer parts are bluer than those in



the inner parts by 0.01 magnitudes, but a Mann-Whitney test shows that this difference is not statistically significant.

One might be concerned that the gradient in the S0 population is driven by the radially increasing fraction of blue outliers. We tested the effect of outliers by excluding from the analysis the S0 galaxies that are more than 0.1 magnitudes bluer than the CM relation. We stress that since we have full membership information there is no justification for removing the blue outliers from the sample, other than to test whether these galaxies drive the trends with radius. The trend in the S0 colors proved to be very similar for  $R < 150''$ . The scatter in the outermost bin goes down from 0.046 to 0.031 when the four blue outliers in this bin are removed, indicating that the scatter in individual radial bins has considerable uncertainty. The robustness of the trends in the scatter and the mean color demonstrate that the scatter and mean color are a good approximation to the width and location of the CM ridge line. Our results therefore describe the bulk of the population, and are not unduly influenced by a small interfering population.

We tested whether the trends with radius of the S0 galaxies could be caused by the misclassification of a few early-type spirals as S0s in the outer part of the cluster. Assuming a scatter of 0.021 for the S0 population, and a three times larger scatter for Sa galaxies, we find that  $\sim 55\%$  of the S0 galaxies in the outer parts of the cluster must be misclassified spirals to explain the observed scatter of 0.043 magnitudes. We conclude that our conclusions are robust against the misclassification of a few spirals as S0s.

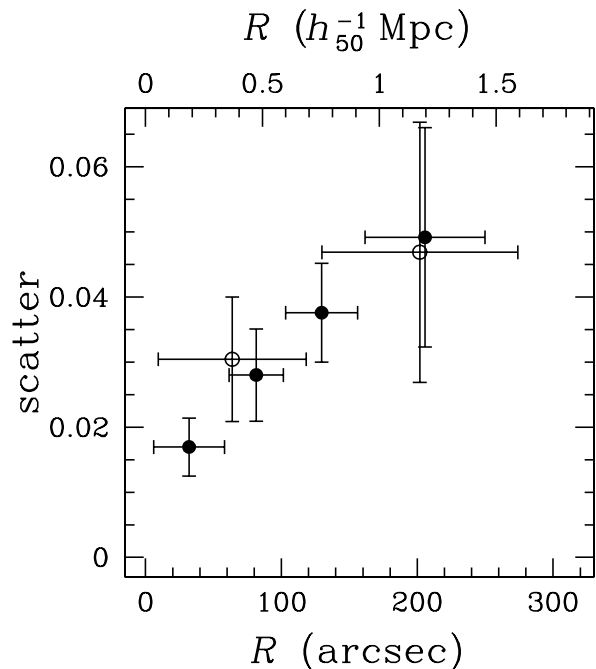


Fig. 10.— The dependence of the scatter in the CM relation on  $R$ , the distance from the BCG, for early-type galaxies with  $n = 3$  (solid circles), and  $n = 1, 2$  (open circles), with  $n$  the value that gives the lowest  $\chi^2$  in profile fits of the form  $r^{1/n}$ . The  $n = 3$  galaxies often have strong bulges. The trend with  $R$  of the  $n = 3$  galaxies is very similar to the trend of the  $n \leq 2$  galaxies. This shows that the trend of the colors of the S0 galaxies with  $R$  is not driven by bulge-to-disk ratio.

We also tested whether the gradient in color and scatter in

the CM relation is caused by a gradient in bulge-to-disk ratio: it may be that there are more disk dominated galaxies in the outer parts of the cluster, and that the disks are bluer than the bulges. When we subdivide our sample by best fitting profile parameter  $n$ , we find that the gradients are independent of  $n$ , for  $n \leq 4$ . In particular, the trends with  $R$  are very clear in the  $n = 3$  galaxies, which have significant bulges. In Fig. 10, the radial trend of the scatter in the CM relation is plotted for galaxies classified as early-type with  $n = 3$  (solid circles), and  $n \leq 2$  (open circles). The colors of the S0 galaxies with strong bulges ( $n = 3$ ) depend similarly on  $R$  as the colors of S0s with weak bulges ( $n \leq 2$ ). This result strongly suggests that both bulges and disks are responsible for the color differences. We return to this issue in Sect. 4.

We investigated whether either the red or blue galaxies are located in subclumps. Figure 11 shows the spatial distributions of the S0s in various color bins. For comparison, the spatial distribution of the ellipticals is also shown. The differences between the spatial distributions of the various subsamples are striking. The blue S0s avoid the cluster core, and their spatial distribution does not appear relaxed. There seem to be more mildly blue S0s to the West of the cluster center than to the East. These results confirm that the S0 galaxies in the core are redder than the S0 galaxies in the outskirts of the cluster.

We conclude that the differences between the CM relations of the ellipticals and the S0 galaxies discussed in the previous Section are caused by the increased scatter and bluer colors of the S0s in the outer part of the cluster. The S0s in the inner parts follow a similar CM relation as the ellipticals, whereas those in the outer parts have characteristics indicative of more recent, or more intense, star formation. We cannot exclude a small ( $\leq 0.01$ ) trend of the elliptical colors with radius, but the trend of the S0 colors is much more significant. These are the key observational results of the paper; they are discussed more extensively below.

#### 4. BLUE BULGES AND DISKS

It is natural to expect that the color differences between S0 galaxies are caused in a large part by blue disks, as it is usually assumed that star formation in disks lasts much longer than star formation in bulges. Some bulge dominated galaxies also show blue colors, hence the process must be more complex. The high resolution of our HST data allows us to study the radial color gradients in the S0 galaxies, and to directly test if the central parts behave differently than the outer parts.

As a first test, we determined the colors within  $0.5 r_e$ , instead of the  $1 r_e$  used above. The color changes going to a smaller aperture do not appear correlated with radius in the cluster. We then examined the full color profiles of our sample galaxies. In general, the color gradients within the galaxies are small, but we find some galaxies with disks that are considerably bluer than their bulges or the reverse.

We show three typical color profiles in Fig. 12(c). Color images of these galaxies are shown in Fig. 4 [Plate 4]. The radial surface brightness profiles of the galaxies are shown in Fig. 12(a). These profiles were determined from the deconvolved images with the GALPHOT package (Franx, Illingworth, & Heckman 1989). The top profile in Fig. 12(c) is a normal S0 on the CM relation, the middle profile is an S0 which is slightly blue, and the bottom profile is a very blue S0. Clearly, these color profiles do not show large radial changes.

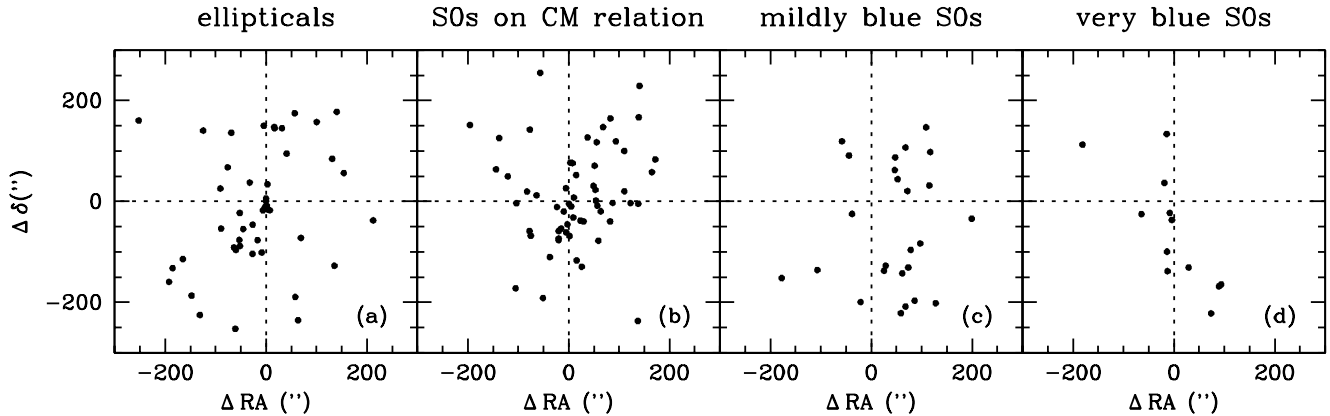


Fig. 11.— The spatial distributions of the ellipticals (a), and the S0s in various color bins (b-d). In (b), the distribution of S0s within  $0.021$  magnitudes (the  $1\sigma$  scatter in the CM relation of the S0s in the inner parts of the cluster) of the CM relation is shown. In (c), mildly blue ( $-0.10 < \Delta(B-V)_z < -0.021$  are shown, where  $\Delta(B-V)_z$  is the distance to the CM relation) S0s are shown, and (d) shows the distribution of very blue S0s ( $\Delta(B-V)_z \leq -0.10$ ). The distributions of the various subsamples are very different. In contrast to the S0s on the CM relation, the mildly blue S0s avoid the cluster core.

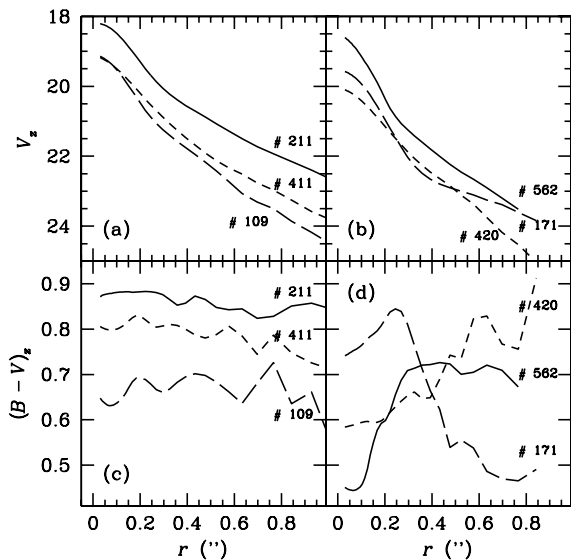


Fig. 12.— Radial surface brightness profiles (a,b) and color profiles (c,d) of early-type galaxies in CL 1358+62. In (a) and (c), surface brightness profiles and typical color profiles of an S0 galaxy on the CM relation (211), a mildly blue S0 (411), and a very blue S0 (109) are shown. The color gradients of these S0 galaxies are very similar, indicating that both the bulges and the disks of the blue S0s contain young populations. The majority of the blue S0s have shallow color gradients. In (b) and (d), examples of galaxies with extreme color gradients are shown: two galaxies with blue bulges compared to their disks (420 and 562), and a galaxy with a blue disk compared to its bulge (171). Images of the galaxies in this Figure are shown in Fig. 4 [Plate 4].

Although the color differences between the bulges and the disks are small for most galaxies, some galaxies do have large

color gradients. In particular, some of the bluest early-type galaxies have very blue bulges. In Fig. 12 (d) three examples of galaxies with extreme color gradients are shown. One has a blue disk, two have blue bulges. Images of the galaxies are shown in Fig. 4 [Plate 4]. At all radii these galaxies are bluer than galaxy 211, which falls on the CM relation.

We conclude that the trends in the S0 colors with distance from the BCG cannot solely be attributed to prolonged star formation in the disks of the S0s in the outer part of the cluster. Although there are a few galaxies with blue disks and red bulges, most S0 galaxies have small color gradients, implying that the bulges were affected as much as the disks, or that the star formation was stronger in the centers of the disks. Interestingly, we find that some of the bluest galaxies have very blue bulges compared to their disks.

##### 5. ARE THERE LUMINOUS BLUE GALAXIES ?

Fig. 6 demonstrates that the brightest galaxies in CL 1358+62 are all red. There are no galaxies that are more than  $0.1$  magnitudes bluer than the CM relation among the brightest 29 galaxies in the sample. Their low scatter in color suggests that the population of bright galaxies is very stable between  $z = 0.33$  and  $z = 0$ . The relatively low luminosity of the bluest galaxies has been noticed before in other clusters (e.g., Butcher & Oemler 1984, Thompson 1986).

Interestingly, the distribution along the ridge line of the CM relation of the bright S0 galaxies also seems tighter than that of the less luminous S0s. Also, judging from Fig. 7 it appears that the radial behavior of the colors of the brightest S0s is more similar to that of the ellipticals than to that of the fainter S0s, although the numbers are small.

We measured the scatter and offset of the CM relation of the brightest one third of the S0 galaxies ( $V_z < 20.52$ ). The scatter in this sample is  $0.019 \pm 0.003$ , and the offset  $-0.003 \pm 0.004$ . These values are similar to the scatter and offsets of the ellipticals (cf. Table 2) and of the S0s in the inner part of the cluster. The scatter for the bright S0s is significantly different from that

of the whole S0 sample. Furthermore, the S0s with  $V_z < 20.52$  do not show the strong trend with radius that is evident for the whole S0 sample. The scatter for the bright S0s at  $R > 118''$  is  $0.021 \pm 0.004$ , and the offset  $-0.010 \pm 0.005$ . The scatter for the complete S0 sample in the outer parts is much higher, at  $0.043 \pm 0.009$ .

Although the brightest galaxies are generally very red, there are a few luminous early-types that are slightly bluer than the average CM relation. As an example, galaxy 233 is the 8th brightest galaxy in the sample, and is 0.04 magnitudes bluer than the CM relation. It is classified as an elliptical, and it is best fitted by a de Vaucouleur  $r^{1/4}$ -law. (see Fig. 4 [Plate 4]). It may be that the brightest galaxies in the cluster have had a different star formation history than the bulk of the cluster population, e.g., they may have had their star formation turned off at earlier times. The presence of a few bright galaxies with slightly bluer colors suggests that we may find luminous blue early-types in clusters at higher redshifts.

## 6. IMPLICATIONS FOR THE STAR FORMATION HISTORIES

In this Section, we construct a range of models for the star formation histories of the ellipticals and the S0s. The aim is to constrain the most recent period of star formation in the ellipticals and the S0s from the observed scatter in the CM relation. We assume that the scatter in the CM relation arises from age differences among the galaxies. The fact that essentially all early-type galaxies that are more than 0.1 magnitudes bluer than the CM relation have strong Balmer absorption lines (Fisher et al. 1997) supports this interpretation.

### 6.1. Models

While the usual assumption is that most of the star formation in early-type galaxies occurred in single bursts, there is good evidence that many galaxies in clusters have more complicated star formation histories. The spectra of blue galaxies in intermediate  $z$  clusters can be fit by models that incorporate truncated star formation in disks, or secondary bursts of star formation in spirals or ellipticals (e.g., Couch & Sharples 1987, Poggianti & Barbaro 1996, Barger et al. 1996).

Motivated by these studies, we consider three scenarios: 1) formation of all the stars in a galaxy in a single burst of star formation, 2) formation of the bulk of the stars in a first burst, followed by a second burst of star formation involving a small fraction of the mass of the galaxy, and 3) a truncated uniform star formation rate. We use simple semi-analytical descriptions of the color evolution to predict the scatter in the CM relation. The derivation of the color evolution is given in Appendix A for each of the models.

The purpose of the modeling is to compare the model predictions to the observed scatter in the CM relation, under various assumptions. We focus on the scatter in the CM relation of the ellipticals and of the S0s in the outer parts of the cluster, since the scatter in the CM relation of the S0s in the inner parts is very similar to that of the ellipticals. The intrinsic scatter for the ellipticals is 0.022 magnitudes, and for the S0s in the outer parts of the cluster 0.042 magnitudes (cf. Table 2). A small (10%) correction must be made to the intrinsic scatter because the increased luminosity of young galaxies artificially increases the scatter in the CM relation (cf. Appendix B). The corrected intrinsic scatter is 0.020 magnitudes for the ellipticals, and 0.038 for the S0s in the outer parts of the cluster.

## 6.2. Application of the Models to the Data

### 6.2.1. Constraints on the Most Recent Period of Star Formation

The scatter in the CM relation only constrains the scatter in the relative ages of the galaxies, and not the absolute ages (see Bower et al. 1992b, Appendix A). The galaxies could have an arbitrarily low mean age, provided that their formation was sufficiently synchronized. It is not possible to determine the most recent period of star formation from the models without making further assumptions.

To break this degeneracy, we assume simple top hat probability distributions in time for the star formation events that characterize the models (single bursts, secondary bursts, truncation of uniform star formation). In Sect. 6.2.2 we will investigate the effects of relaxing this assumption. In the single burst model, galaxies form in a  $\delta$ -peak at a random time. In the secondary burst model, 80% of the mass of the galaxies forms in a burst at  $t = 0$ , and 20% in a second burst at a random time. In the truncated star formation model, the star formation starts at  $t = 0$  for all galaxies, continues at a constant rate, and terminates at a random time.

The models are schematically represented in Fig. 13 and Fig. 14. The scatter in the CM relation of the ellipticals is reproduced in Fig. 13, and that of the S0s in the outer part of the cluster in Fig. 14. The bottom panels in Fig. 13 and Fig. 14 show the histograms of the residuals from the CM relation, derived from Monte-Carlo simulations with 5000 galaxies. The scatter and offset of these simulated distributions are measured in the same way as the observed parameters.

The scatter of 0.020 in the colors of the ellipticals can be reproduced by the three models (Fig. 13). In the single burst model, the youngest ellipticals formed at  $z = 1.2$ . In the secondary burst model, the most recent bursts occurred at  $z = 0.5$ . In the truncated star formation model, the youngest ellipticals were forming stars up to  $z = 0.6$ . The constraints on the most recent period of star formation thus depend on the assumed model for the star formation history. In particular, in the truncated star formation model the ages of the most recently formed galaxies are a factor of 2 lower than in the single burst model. This generic feature of the models can be derived analytically (cf. Appendix A).

The scatter in the colors of the S0s can be reproduced by the single burst model and the truncated star formation model (Fig. 14). In the single burst model, the youngest S0s formed at  $z = 0.7$ . The secondary burst model predicts a scatter of 0.035, if the mass fraction involved in the burst is 20% and the bursts occur continuously up to  $z = 0.33$ . This is slightly lower than the observed scatter. Stronger bursts (involving mass fractions of  $\sim 25\%$ ) are required to explain the observed scatter with this model. The truncated star formation model can reproduce the observed scatter if the youngest S0s were forming stars up to  $z = 0.33$ , the redshift of the cluster.

An important result is that all three models allow for quite recent star formation in the S0s in the outer part of the cluster. The formation time of the galaxies is pushed back furthest in the single burst model, but even in this model the youngest S0s formed as recently as  $z \sim 0.7$ .

### 6.2.2. Other Probability Distributions

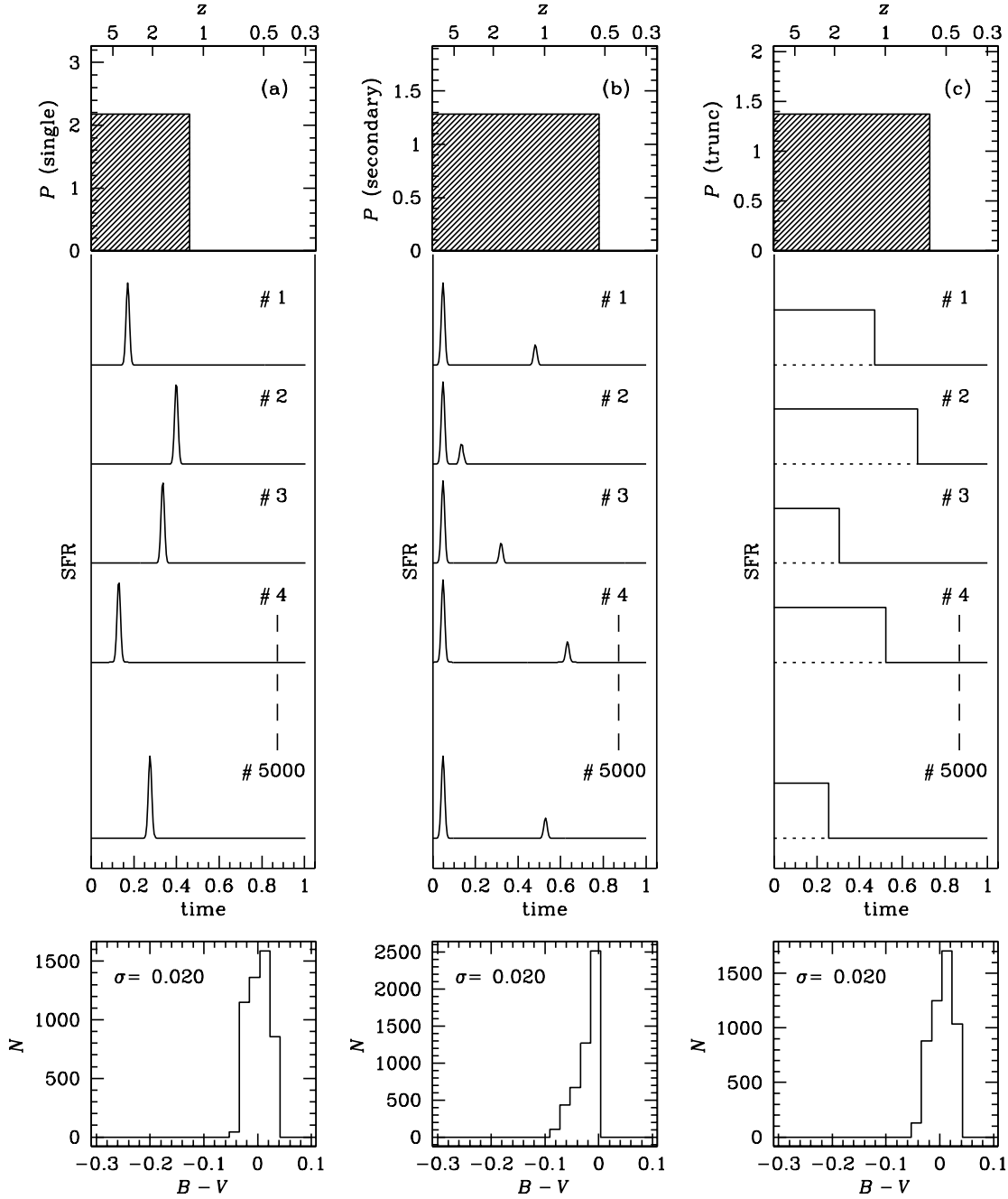


Fig. 13.— Reproduction of the scatter in the CM relation of the ellipticals (0.020) in three different models. In (a), galaxies form in a  $\delta$ -peak at a random time between  $t = 0$  and  $t = 0.46$  ( $z = 1.2$ ;  $q_0 = 0.5$ ). In (b), 80% of the mass of the galaxies forms in a single burst at  $t = 0$ , and 20% of the mass in a second burst at a random time between  $t = 0$  and  $t = 0.78$  ( $z = 0.5$ ). In (c), the galaxies start forming stars at  $t = 0$  and stop forming stars at a random time between  $t = 0$  and  $t = 0.73$  ( $z = 0.6$ ). Note that  $t$  is scaled such that  $t = 1$  corresponds to  $z = 0.33$ . The top panels show the probability distributions  $P$  for the events that characterize the models (single bursts, secondary bursts, truncation of star formation). The model color distributions at  $z = 0.33$  are shown in the bottom panels, derived from Monte Carlo simulations with 5000 model galaxies. The constraints on the last period of star formation are very dependent on the model for the star formation history.

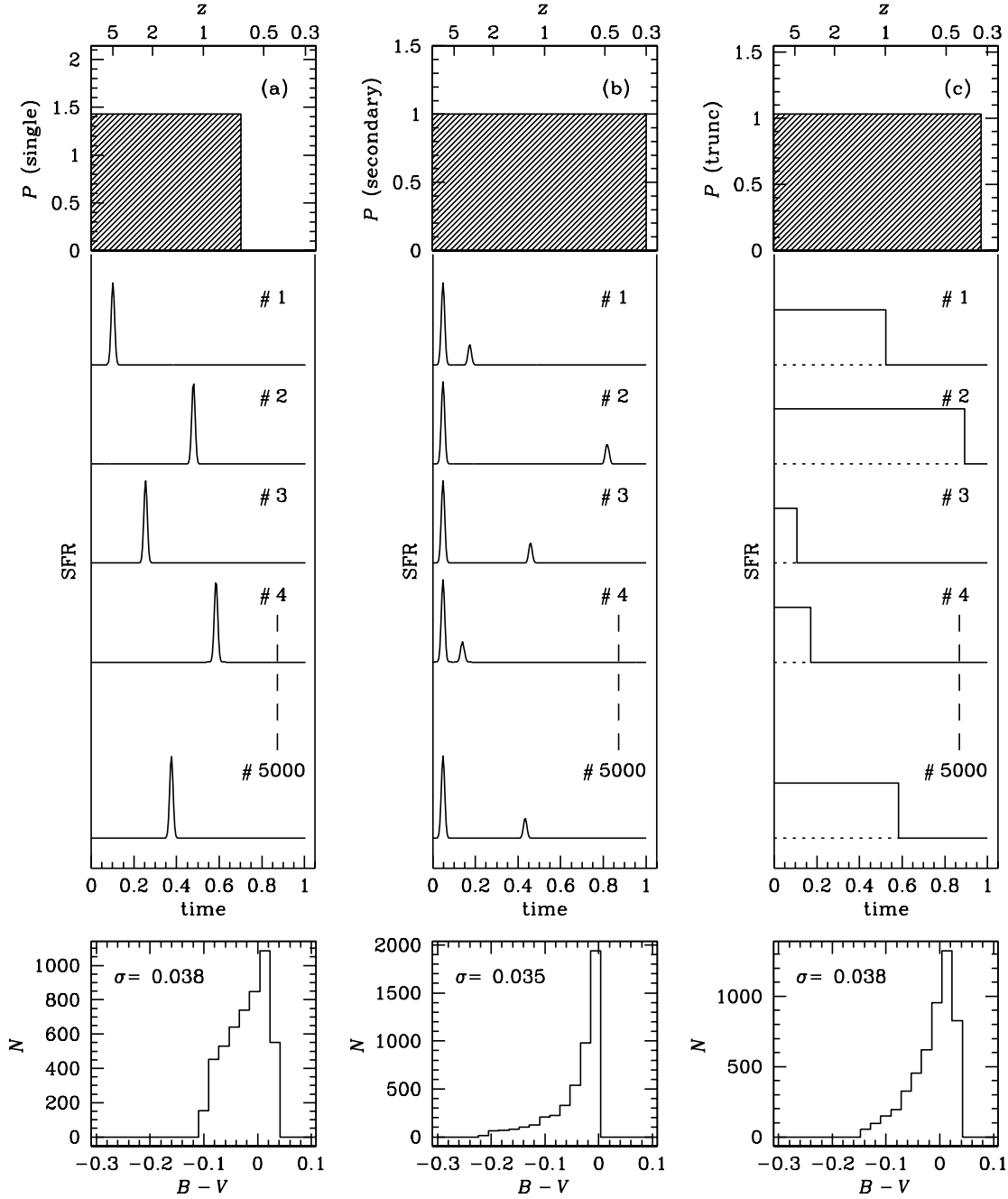


Fig. 14.— Reproduction of the scatter in the CM relation of the S0 galaxies in the outer parts (0.038) in three different models. In the single burst model, the youngest S0s formed at  $z \approx 0.7$  (a). Secondary bursts involving 20% of the mass that occur from  $t = 0$  to the epoch of observation (b) predict a scatter that is somewhat lower than what is observed. The truncated star formation model (c) can reproduce the observed scatter if the youngest S0s were forming stars up to  $z = 0.33$ , the redshift of the cluster.

The assumption in the preceding Section is that the probability distributions for the star formation events that characterize the models are simple top hats. Here, we investigate how stable our conclusions are when this assumption is relaxed. We consider two other probability distributions: an exponentially decreasing probability distribution, and a Gaussian. For simplicity, only single burst models are considered, and only the scatter in the ellipticals and the S0s in the core of the cluster is reproduced.

In Fig. 15 three probability distributions are shown that reproduce the scatter in the ellipticals and S0s in the core of CL 1358+62. The exponential distribution has the form  $P = e^{-5t/t_{0.33}}$ , where  $t_{0.33}$  is the age of the universe at  $z = 0.33$ . The mean of the Gaussian is at  $z = 2$ , and the width is  $0.13t_{0.33}$ .

The formation time of the youngest galaxies is more difficult to define for other distributions than the top hat, since the Gaussian and exponential distribution have a tail extending to infinity. We calculated when 50% and 75% of the galaxies have formed assuming the three distributions (top hat, exponential, and an example of a Gaussian). The open dots indicate the time when 50% of the galaxies have been formed, and the solid dots indicate the time when 75% of the galaxies have been formed. In all the models  $\sim 25\%$  of the ellipticals and the S0 galaxies in the core of the cluster formed after  $z = 2$ . This is a generalization of the result that the youngest ellipticals and S0 galaxies in the core of the cluster formed at  $z \sim 1.2$ , which was derived for the top hat model in the previous Section.

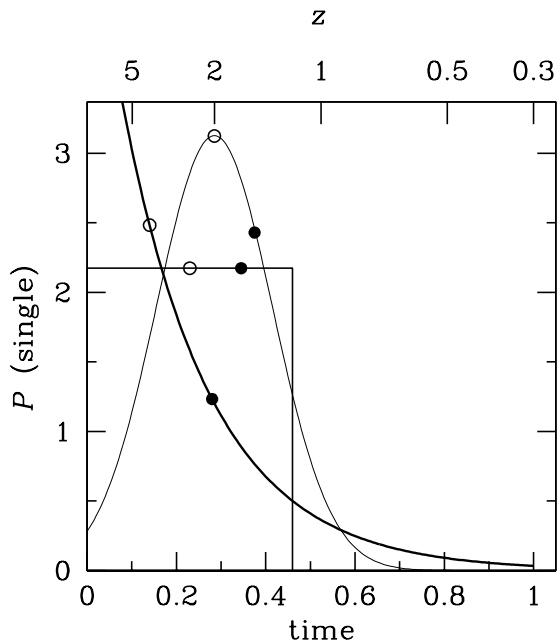


Fig. 15.— Three probability distributions for galaxy formation in single bursts of star formation that reproduce the observed scatter in the CM relation of the S0 galaxies in the core and the elliptical galaxies in CL 1358+62. Open dots indicate the times when 50% of the galaxies have been formed, in each of the models. Solid dots indicate the times when 75% of the galaxies have been formed.

Similar to the top hat distribution, the exponentially decreasing probability distribution has one free parameter, and is therefore fully determined by the observed scatter at  $z = 0.33$ . The Gaussian distribution has two free parameters: any Gaus-

sian distribution that satisfies the constraint  $\sigma_t/(t_{0.33}-t') = 0.18$ , where  $\sigma_t$  is the width of the Gaussian and  $t'$  is the mean, reproduces the observed scatter in the CM relation for the ellipticals and the S0s in the core of the cluster. We note that the Gaussian distribution has the general property that it allows for more recent star formation than the top hat or the exponential. In particular, the time when 75% of the galaxies have been formed is always after  $z = 2$ , for any combination of  $\sigma_t$  and  $t'$ .

### 6.2.3. Constraints on the Scatter in the Luminosity Weighted Age

The constraint on the most recent period of star formation is very dependent on the model that is assumed for the star formation history (cf. Sect. 6.2.1). In particular, models with truncated continuous star formation allow for much later star formation than single burst models. Here, we investigate how well we can constrain the scatter in the mean ages and the mean luminosity weighted ages of the galaxies.

The scatter in the mean ages of the galaxies is also rather model dependent. In the models described in Sect. 6.2.1,  $0.05 < \Delta\tau/\langle\tau\rangle < 0.20$  for the ellipticals, and  $0.07 < \Delta\tau/\langle\tau\rangle < 0.35$  for the S0s in the outer parts of the cluster. This large range results from the fact that the color of a galaxy is mostly determined by the youngest stars that contribute most of the light.

The scatter in the V band luminosity weighted ages is better constrained. The expressions for the luminosity weighted ages  $\tau_L$  for each of the models are given in the Appendix. For the ellipticals, the single burst model gives  $\Delta \ln \tau_L = 0.18$ , the truncated star formation model  $\Delta \ln \tau_L = 0.16$ , and the secondary burst model  $\Delta \ln \tau_L = 0.13$ . For the S0s in the outer parts, we find  $\Delta \ln \tau_L = 0.35$  in the single burst model, and  $\Delta \ln \tau_L = 0.30$  in the truncated star formation model.

Secondary burst models provide the strongest constraints on the scatter in the luminosity weighted ages; weaker but similar constraints are provided by the single burst model and in the truncated star formation models. The constraints on  $\Delta \ln \tau_L$  are not very dependent on the distributions of the formation times and truncation times. The various probability distributions discussed in Sect. 6.2.2 give very similar results as the top hat distributions of Sect. 6.2.1. We consistently find  $\Delta \ln \tau_L < 0.18$  for the ellipticals, and  $\Delta \ln \tau_L < 0.35$  for the S0s in the outer part of the cluster. Since  $\Delta \ln \tau_L = \Delta\tau_L/\langle\tau_L\rangle$ , these numbers are a combined constraint on the spread in ages of the galaxies, and the mean age of the galaxy population.

## 7. EVOLUTION OF THE SCATTER IN THE CM RELATION

All of the models discussed in the previous Section reproduce the observed scatter in the CM relation of the ellipticals and S0s at  $z = 0.33$ . These models make very different predictions for the scatter in the CM relation at other redshifts. Therefore, in principle, the models can be constrained by observations of the scatter in the CM relation at different redshifts. In this Section, the predictions from the models discussed in Sect. 6.2.1 are compared to data from the literature on the central regions of the Coma cluster at  $z = 0.02$ , and the central regions of three clusters at  $z \sim 0.55$ . At present, there is no data available in the literature for the scatter in the CM relation of early-type galaxies in the outskirts of clusters, where we measure the high scatter for the S0 galaxies.

Figure 16(a,b) shows the predictions of the single burst and truncated star formation models in Sect. 6.2.1 for the evolu-

tion of the scatter in the CM relation with redshift. Predictions for the ellipticals and the S0s in the outer part of the cluster are shown. Note that the scatter is constant with time while the galaxies were being formed. For *any* continuous formation process the scatter is constant because it arises from  $\Delta\tau/\langle\tau\rangle$ , and the mean age of the galaxies increases at the same rate as the scatter in the ages. After the end of the formation phase of the galaxies, the scatter decreases monotonically, because the relative age differences between the galaxies become smaller. Therefore, a nearly constant scatter in the CM relation with redshift, such as observed by Stanford et al. (1997), implies that the galaxies either formed at very high redshift, or that galaxies are continuously formed and added to the sample.

For the ellipticals, it is not possible to distinguish between the truncated star formation model and the single burst model at  $z \lesssim 0.8$ . For the S0s in the outer parts, the predictions of the single burst model and the truncated star formation model discussed in Sect. 6.2.1 are already a factor two different at  $z \geq 0.6$ . Note that the scatter at  $z = 0$  is not well constrained in the truncated star formation model (the broken line in Fig. 16b). The constraint is weak because the S0s are still forming at  $z = 0.33$ : the scatter may be as low as 0.015 at  $z = 0$  if the production of S0s stops at  $z = 0.33$ , or remain constant at  $\sim 0.040$  if the formation continues up to the present epoch.

The solid symbols indicate the observed scatter in the ellipticals (Fig. 16a) and the S0s in the outer parts of the cluster (Fig. 16b) at  $z = 0.33$ . The open symbols in Fig. 16(a) are derived from data for the central regions of the Coma cluster by Bower, Lucey, & Ellis (1992a,b), and from the Ellis et al. (1997) study of the CM relation in the cores of three clusters at  $z \sim 0.55$ . The Bower et al. (1992a) and Ellis et al. (1997) data are in restframe  $U - V$ . The color evolution in  $U - V$  is a factor 1.5–2.5 stronger than in  $B - V$ , depending on the metallicity (Worthey 1994). The  $U - V$  data were transformed to  $B - V$  through  $\Delta U - V = 2\Delta B - V$ .

As can be seen in Fig. 16(a), the measurements of the scatter at  $z = 0.02$  and at  $z = 0.55$  are consistent with the model predictions. The measurements we plot in Fig. 16(a) between  $z = 0$  and  $z = 0.55$  are in apparent conflict with Stanford et al. (1997), who found that the scatter in the “blue – red” (roughly  $U - V$ , cf. Stanford et al. 1997) CM relation in the cores of clusters out to  $z \sim 0.9$  is approximately constant with redshift, at  $\sim 0.07$ , or equivalent to  $\sim 0.03$  in  $B - V$ . The model predictions range from 0.02 at  $z = 0.3$  to 0.045 at  $z = 0.9$ . However, judging from Fig. 6 in Stanford et al. (1997), their error bars are consistent with the modest increase in the scatter shown in Fig. 16(a).

We cannot compare our results for the scatter in the CM relation of the S0s in the outer part of the cluster to the above mentioned studies, since they do not extend far enough in radius ( $R \sim 0.6h_{50}^{-1}$  Mpc, compared to  $R = 1.6h_{50}^{-1}$  Mpc for our dataset). At present, large field photometric studies of the Coma cluster (e.g., Godwin et al. 1983, Mazure et al. 1988) are not sufficiently accurate to allow a meaningful comparison with the high  $z$  studies of the CM relation. Large field ground based studies of intermediate redshift clusters such as that of Abraham et al. (1996b) lack the resolution to determine galaxy morphologies, and sufficiently accurate colors. Our results, and those of Caldwell et al. (1993) for the Coma cluster, suggest that it may be of interest to extend accurate studies of the scatter in the CM relation of early-types to larger radii, at high and low redshift.

## 8. INFALL AND THE PROGENITORS OF PRESENT-DAY EARLY-TYPES

There is good evidence that many clusters of galaxies have significant substructure (e.g., Forman et al. 1981, Geller & Beers 1982, Dressler & Shectman 1988, White, Briel, & Henry 1993). This is consistent with theoretical predictions: it is expected that clusters accrete a significant amount of mass after their initial collapse (e.g., Gunn & Gott 1972, Evrard 1990, 1991, Frenk et al. 1996). During the accretion, it is likely that galaxies are transformed from star forming galaxies into non-star forming galaxies, to produce the passively evolving galaxies that are observed in rich clusters. The galaxies in which the star formation has been shut off will be observed as blue, non-star forming galaxies for a short period ( $\sim 1$  Gyr). These galaxies are expected to be more abundant in the outskirts of the cluster (Evrard 1991; Frenk et al. 1996). The blue early-type galaxies that we observe in CL 1358+62 may therefore be recently accreted galaxies that have had their formation terminated upon entry.

The accretion process may be related to the Butcher-Oemler effect (e.g., Dressler & Gunn 1983, Butcher & Oemler 1984, Lavery & Henry 1994, Moore et al. 1996, Abraham et al. 1996b). It is often suggested that the Butcher-Oemler effect is caused by an enhanced accretion at higher redshifts (e.g., Kauffmann 1995). The cluster CL 1358+62 displays a mild Butcher-Oemler effect (Luppino et al. 1991; Fabricant et al. 1991), and it will be interesting to see whether the scatter of the early-type galaxies in the outer parts correlates with the Butcher-Oemler effect.

If galaxies are accreted from the field, with a subsequent cut-off in their star formation rate, then the set of non-star forming galaxies in clusters evolves with time. Hence the non-star forming galaxies at  $z = 0.33$  are a subsample of the non-star forming galaxies at  $z = 0$ , for the same cluster. This evolution makes it harder to compare samples of early-type cluster galaxies at different redshifts: at high redshift there will be an observational bias towards the oldest progenitors of present day early type galaxies.

We calculate the importance of this effect by estimating the number of galaxies that will be added to the early-type galaxy population between  $z = 0.33$  and  $z = 0$ . The subsample that is consistent with continuous accretion (the S0s in the outer parts of the cluster) comprises about 1/3 of the early-type galaxy population of CL 1358+62. This implies that the accretion rate must have decreased considerably since the onset of the formation of the cluster, which is consistent with theoretical predictions (e.g., Lacey & Cole 1993, Kauffmann 1995). If we assume that the accretion rate remains constant after  $z = 0.33$ , we obtain an upper limit on the accreted and transformed fraction. For  $q_0 = 0.5$  we derive that only  $\sim 15\%$  of the early-type galaxy population at  $z = 0$  has been added after  $z = 0.33$ . The main uncertainty is the limited field of view of our data.

The transformation rate is smaller when only bright galaxies are considered. As discussed in Sect. 5, the bluest galaxies have low luminosities. The most massive galaxies were therefore probably transformed into passively evolving systems at earlier times. It is difficult to add young bright galaxies to the cluster sample, even when we consider mergers. The merger of the two brightest galaxies that are more than 0.10 magnitudes bluer than the CM relation would produce a galaxy of  $V_z \sim 19.3$ . This galaxy would be placed among the brightest galaxies in CL 1358+62, but only for a short time. The luminosity of such

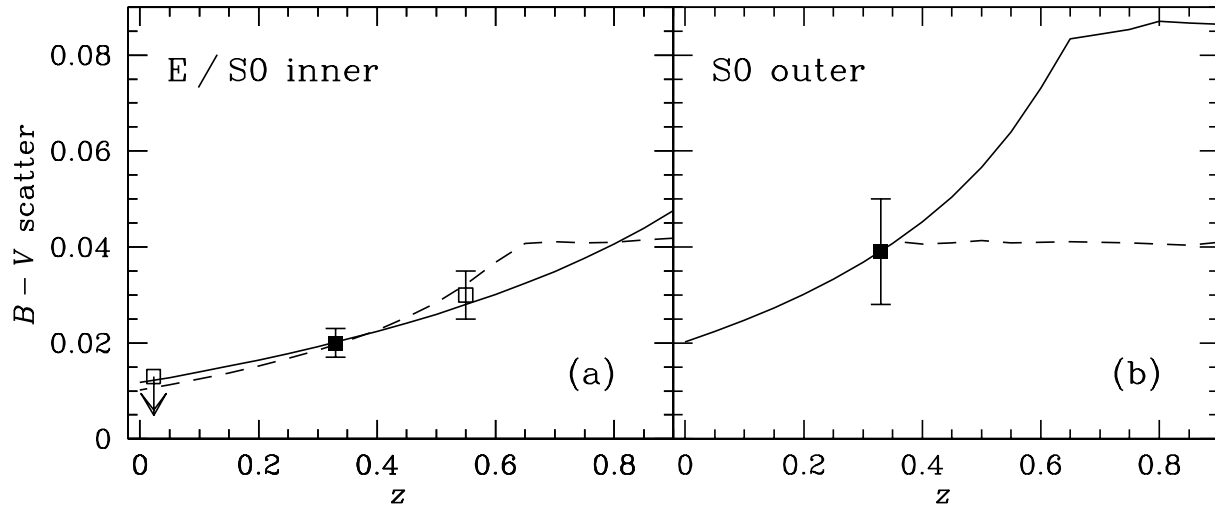


Fig. 16.— The evolution of the scatter in the CM relation. Solid symbols indicate the observed scatter of the ellipticals in CL 1358+62 (a), and of the S0s in the outer parts of CL 1358+62 (b). Open symbols in (a) represent the ellipticals in the core of the Coma cluster at  $z = 0.02$  from Bower et al. (1992), and the ellipticals and S0s in the cores of three clusters at  $z = 0.55$  from Ellis et al. (1997), transformed to restframe  $B-V$ . The lines are the predictions from the models discussed in Sect. 6.2.1. The models in (a) reproduce the scatter in the CM relation of the ellipticals in CL 1358+62, and of the S0s in the inner parts. The models in (b) reproduce the scatter of the S0s in the outer parts of CL 1358+62. Solid lines are single burst models, broken lines are truncated continuous star formation models (cf. Sect. 6.2.1). In the truncated star formation model of (b), the S0s are still forming at  $z = 0.33$ . Therefore, the scatter in the CM relation between  $z = 0$  and  $z = 0.33$  is not well constrained in this model.

a blue galaxy would be expected to fade by  $\sim 0.7$  magnitudes, and the implication is that we have not (yet) observed the young progenitors of massive galaxies.

## 9. SUMMARY AND CONCLUSIONS

We have studied the color-magnitude relation in the rich cluster CL 1358+62 at  $z = 0.33$ . The elliptical galaxies in CL 1358+62 form a very homogeneous population: the observed scatter in the  $B-V$  CM relation is only 0.024 magnitudes, and there is no evidence for an increase in the scatter with distance from the cluster center. We cannot presently exclude a small ( $\lesssim 0.01$  magnitudes) trend in the mean color of the ellipticals.

The S0s are a more heterogeneous population. The scatter and the mean color of the CM relation are strong functions of galaxy distance from the cluster center. The CM relations of the ellipticals and the S0s in the inner parts of the cluster are very similar, as is the case for three clusters at  $z \sim 0.55$  studied by Ellis et al. (1997). The S0s in the outer parts of CL 1358+62 are bluer by 0.02 magnitudes, and have a larger scatter than the S0s in the inner parts (0.043 vs. 0.021). Fig. 11 demonstrates that the mildly blue S0s avoid the cluster core. The morphologies of the mildly blue S0s are very similar to those of the red S0s (cf. Fig. 4 [Plate 4]). The very blue S0s generally have low luminosities.

The systematic bluing of the CM relation with radius has been observed before (in the cluster Abell 2390 at  $z = 0.23$ , by Abraham et al. 1996b), but this is the first time that the morphologies of the galaxies at large distances from the cluster center could be determined. Also, the colors in the study of

Abraham et al. (1996b) are not accurate enough for the detection of the radial gradient in the scatter in the color-magnitude relation.

We have constructed a range of models to explain the scatter in the CM relation of the ellipticals and the S0s in the outer parts of the cluster. We find that truncated continuous star formation models allow for more recent star formation than single burst models. The youngest ellipticals formed before  $z = 1.2$  if they formed in single bursts of star formation, and before  $z = 0.6$  if they experienced a constant star formation rate until an abrupt truncation. In all models, the youngest S0s in the outer parts of the cluster formed stars until close to the epoch of observation. In the truncated star formation model, star formation in these galaxies continued until the epoch of observation.

The radial trend of the S0 colors is consistent with the hypothesis that galaxies and groups are continuously accreted from the field. In this picture, the blue S0s are the galaxies that have been accreted recently. The star formation in the infalling galaxies is turned off upon entering the cluster. The truncation of the star formation may be accompanied by a small starburst in the nucleus (e.g., Hernquist & Mihos 1995). This nuclear starburst would explain the blue bulges (and the small color gradients) that we see in many of the blue S0 galaxies (cf. Sect. 4). The accretion radius of the cluster is roughly  $3 h_{50}^{-1}$  Mpc (Carlberg, Yee & Ellingson 1997), which is just outside our HST mosaic. If the morphological transformation between spirals and S0s occurs before accretion into the denser regions of the cluster, while the galaxies are still in small groups, that process probably occurs at radii beyond the limit of our observations. This might explain the small fraction of spirals in this very rich cluster.



The continuous infall of field galaxies implies that the fraction of non-star forming galaxies in clusters evolves with time. This complicates the comparison between galaxy populations in high redshift clusters and local clusters. Assuming a constant accretion rate after  $z = 0.33$ , we estimate that  $\sim 15\%$  of the present-day early-type galaxy population in clusters has been added between  $z = 0.33$  and  $z = 0$ . We infer that the accretion rate was higher before  $z = 0.33$ , which is consistent with model predictions (e.g., Kauffmann 1995).

The infall and transformation process seems to affect mostly the faint end of the galaxy population: the bluest galaxies have low luminosities. There are a few bright early-types with slightly bluer colors than the CM relation. Their presence suggests that bright early-type galaxies with young populations may be found in clusters at higher redshifts.

The homogeneity of the ellipticals and luminous S0s suggests that their star formation had ceased before they were accreted onto the cluster. There are several possible mechanisms, e.g., the star formation may have ceased after the collapse of smaller subclumps (galaxy groups) in which the galaxies resided. Studies of early-type galaxies in the field will be valuable to determine the process that shuts off the star formation in bright early-types before they enter the cluster environment.

This study demonstrates the need for large field, high resolution observations of distant clusters. If only one HST WFPC2 pointing had been available, our conclusions would be quite different: inside  $R = 80''$ , there is no systematic difference in the scatter or offset of the CM relation for the ellipticals and the S0s. Additional wide field observations are needed to establish whether CL 1358+62 is typical of intermediate  $z$  clusters and to extend this study to higher redshifts. High quality data for nearby clusters extending over a wide field would also be valuable. It will be interesting to explore whether the differences between ellipticals and S0s, and the environmental dependence of the colors, are reflected in the Fundamental Plane of this cluster: the observed scatter of 0.043 in the S0 colors in the outer parts implies a scatter in the Fundamental Plane in the  $V$  band of  $\sim 30\%$  in  $\mu_e$ .

We thank the referee, Dr. Ian Smail, for his constructive comments, which improved the paper. Henk Hoekstra is thanked for a critical reading of the appendix. The University of Groningen and the Leids Kerkhoven-Bosscha Fonds are thanked for support. Support from STScI grants GO05989.01-94A, GO05991.01-94A, and AR05798.01-94A is gratefully acknowledged.

## APPENDIX

### MODELS FOR THE COLOR EVOLUTION

#### *Single bursts*

In this model the galaxies formed in single bursts of star formation at  $t = t_0$ . The luminosity evolution of a single age stellar population can be described by a power law:

$$L \propto \frac{1}{(t-t_0)^\kappa}, \quad (\text{A1})$$

with  $t$  the age of the universe at the epoch of observation, and  $t_0$  the age of the universe at the time of formation of the population. The difference  $t - t_0$  is the age of the population at the epoch of observation. The coefficient  $\kappa$  depends on the passband, but also on the metallicity  $Z$  and the IMF (Tinsley 1980; Worthey 1994).

The color evolution is

$$\frac{L_V}{L_B} \propto (t-t_0)^{\kappa_B - \kappa_V}, \quad (\text{A2})$$

or

$$B - V = 1.086(\kappa_B - \kappa_V) \ln(t-t_0) + C, \quad (\text{A3})$$

where we have set  $B - V \equiv 2.5 \log(L_V/L_B)$ . The evolution of the color depends on the difference  $\kappa_B - \kappa_V$ , which is not very sensitive to differences in  $Z$  or the IMF. The Worthey (1994) models give  $\kappa_B - \kappa_V \approx 0.10$  for  $-2 < Z < 0.5$ . In the single burst model, the scatter in the colors at time  $t$  is proportional to the scatter in  $\ln(t-t_0)$ .

#### *Secondary bursts*

This model is an extension of the single burst model. A mass fraction  $(1-f)$  forms in a burst at  $t = t_0$ , and a mass fraction  $f$  forms in a burst at  $t = t_1$ , with  $t_1 > t_0$ . The luminosity evolves as

$$L \propto \frac{1-f}{(t-t_0)^\kappa} + \frac{f}{(t-t_1)^\kappa}, \quad (\text{A4})$$

and the color as

$$\frac{L_V}{L_B} \propto \frac{(1-f)(t-t_0)^{-\kappa_V} + f(t-t_1)^{-\kappa_V}}{(1-f)(t-t_0)^{-\kappa_B} + f(t-t_1)^{-\kappa_B}}. \quad (\text{A5})$$

Expressed in magnitudes this is

$$B - V \approx 1.086(\kappa_B - \kappa_V) \ln(t-t_0) - 1.086 \frac{f}{1-f} \left[ \left( \frac{t-t_1}{t-t_0} \right)^{-\kappa_B} - \left( \frac{t-t_1}{t-t_0} \right)^{-\kappa_V} \right] + C, \quad (\text{A6})$$

where it is assumed that  $f \ll \frac{t-t_1}{t-t_0}$ , i.e., Eq. A6 is not valid shortly after a strong burst. In that case, the color evolution reduces to the single burst case (Eq. A3), with  $t_0$  replaced by  $t_1$ .

The observed scatter in the colors can be expressed as a constraint on the relevance of star bursts. It is assumed the scatter in the colors is caused by a spread in ages of the bursts only (i.e., not by a spread in  $t_0$  or  $f$ ). Differentiating Eq. A6 with respect to  $(t-t_1)$  gives an expression for the scatter in the colors as a function of the scatter in  $(t-t_1)$ :

$$\Delta(B-V) = 1.086 \frac{f}{1-f} \left[ \kappa_B \left( \frac{t-t_1}{t-t_0} \right)^{-\kappa_B-1} - \kappa_V \left( \frac{t-t_1}{t-t_0} \right)^{-\kappa_V-1} \right] \frac{\Delta(t-t_1)}{t-t_0}. \quad (\text{A7})$$

For  $1.5 < (\kappa_B + \kappa_V) < 2$ , a good approximation to Eq. A7 is

$$\Delta(B-V) \approx 1.086(\kappa_B - \kappa_V) \frac{f}{1-f} \left( \frac{t-t_0}{t-t_1} \right)^{1.5} \Delta \ln(t-t_1). \quad (\text{A8})$$

### Truncated star formation

In this model the galaxies form stars at a constant rate from  $t = t_0$  to  $t = t_1$ . The star formation is truncated at  $t = t_1$ . This model is appropriate for spiral galaxies in which the star formation suddenly terminates. The ages of the stellar populations in the galaxies range from  $(t-t_0)$  to  $(t-t_1)$ . The contribution to the luminosity of each population is  $dt_* (t-t_*)^{-\kappa}$ . Therefore, the total luminosity after  $t = t_1$  is

$$L \propto \frac{1}{t_1 - t_0} \int_{t_0}^{t_1} \frac{dt_*}{(t-t_*)^\kappa}. \quad (\text{A9})$$

The factor  $1/(t_1 - t_0)$  normalizes the mass such that the mass of the galaxy after  $t_1$  is independent of the length of the burst. For  $\kappa_B, \kappa_V \neq 1$  the color evolution is

$$\begin{aligned} \frac{L_V}{L_B} &\propto \frac{1 - \kappa_B}{1 - \kappa_V} \left[ \frac{(t-t_0)^{1-\kappa_V} - (t-t_1)^{1-\kappa_V}}{(t-t_0)^{1-\kappa_B} - (t-t_1)^{1-\kappa_B}} \right] \\ &= \frac{1 - \kappa_B}{1 - \kappa_V} (t-t_0)^{\kappa_B - \kappa_V} \left( \frac{t-t_1}{t-t_0} \right)^{\frac{1}{2}(\kappa_B - \kappa_V)} \frac{\left( \frac{t-t_1}{t-t_0} \right)^{-\frac{1}{2}(1-\kappa_V)} - \left( \frac{t-t_1}{t-t_0} \right)^{\frac{1}{2}(1-\kappa_V)}}{\left( \frac{t-t_1}{t-t_0} \right)^{-\frac{1}{2}(1-\kappa_B)} - \left( \frac{t-t_1}{t-t_0} \right)^{\frac{1}{2}(1-\kappa_B)}}. \end{aligned} \quad (\text{A10})$$

Since

$$\frac{x^{-\alpha} - x^\alpha}{x^{-\beta} - x^\beta} = \frac{\alpha \log x + \sum_{k=2}^{\infty} \frac{1}{(2k-1)!} (\alpha \log x)^{2k-1}}{\beta \log x + \sum_{k=2}^{\infty} \frac{1}{(2k-1)!} (\beta \log x)^{2k-1}} \approx \frac{\alpha}{\beta}, \quad (\text{A11})$$

the color evolution reduces to

$$\frac{L_V}{L_B} \propto \left[ \sqrt{(t-t_0)(t-t_1)} \right]^{\kappa_B - \kappa_V}. \quad (\text{A12})$$

In the truncated star formation model, galaxies are comprised of populations spanning a range of ages. The expression for the color evolution in this model is very similar to that for the color evolution in the single burst model (Eq. A2). However, the rate of evolution is determined by the geometric mean of the ages of the youngest stars and the oldest stars in the galaxy, rather than a single age.

Expressed in magnitudes, Eq. A12 reads

$$B-V = 0.543(\kappa_B - \kappa_V) [\ln(t-t_0) + \ln(t-t_1)] + C. \quad (\text{A13})$$

If it is assumed all galaxies have the same  $t_0$ , the scatter in the  $B-V$  colors at time  $t$  only depends on the scatter in truncation times  $t_1$ .

### Mean ages

Here, we give expressions for the luminosity weighted mean ages  $\tau_L$  in the three models. In the single burst model, all the stars have the same age, and therefore

$$\tau_L = t - t_0. \quad (\text{A14})$$

In the secondary burst model

$$\tau_L = \frac{(1-f)(t-t_0)^{1-\kappa} + f(t-t_1)^{1-\kappa}}{(1-f)(t-t_0)^{-\kappa} + f(t-t_1)^{-\kappa}}, \quad (\text{A15})$$

and in the truncated star formation model

$$\tau_L = \frac{1-\kappa}{2-\kappa} \left[ \frac{(t-t_0)^{2-\kappa} - (t-t_1)^{2-\kappa}}{(t-t_0)^{1-\kappa} - (t-t_1)^{1-\kappa}} \right]. \quad (\text{A16})$$

## CORRECTION FOR LUMINOSITY EVOLUTION

If the scatter in the CM relation is caused by age variations among the galaxies, the observed scatter in the CM relation is partly caused by the increased luminosity of young galaxies. The deviation for a given object in  $B-V$  from the CM relation can be expressed as

$$\Delta(B-V)_{\text{obs}} = \Delta(B-V)_{\text{evo}} - \alpha\Delta V, \quad (\text{B1})$$

where  $\alpha$  is the slope of the CM relation and  $\Delta V$  is the amount of luminosity evolution for a color evolution of  $\Delta(B-V)_{\text{evo}}$ . Since the relation between color evolution and luminosity evolution is

$$\Delta(B-V)_{\text{evo}} = 1.086 \left( \frac{\kappa_B}{\kappa_V} - 1 \right) \Delta V, \quad (\text{B2})$$

with  $\kappa_B, \kappa_V$  defined in Appendix A, it follows that

$$\Delta(B-V)_{\text{obs}} = \left( 1 + \frac{\alpha}{1.086} \frac{\kappa_V}{\kappa_V - \kappa_B} \right) \Delta(B-V)_{\text{evo}}. \quad (\text{B3})$$

The slope of the CM relation  $\alpha = -0.018$  (see Eq. 3). The Worthey (1994) models give  $\kappa_B = 0.90$  and  $\kappa_V = 0.80$  for solar metallicity. These values give a correction for the luminosity evolution of  $\Delta(B-V)_{\text{evo}} \approx 0.90\Delta(B-V)_{\text{obs}}$ .

## REFERENCES

- Abraham, R. G., van den Bergh, S., Glazebrook, K., Ellis, R. S., Santiago, B. X., Surma, P., & Griffiths, R. E. 1996a, *ApJS*, 107, 1
- Abraham, R. G., Smecker-Hane, T. A., Hutchings, J. B., Carlberg, R. G., Yee, H. K. C., Ellingson, E., Morris, S., Oke, J. B., & Rigler, M. 1996b, *ApJ*, 471, 694
- Andreon, S., Davoust, E., & Heim, T. 1997, *a*, 323, 337
- Aragon-Salamanca, A., Ellis, R. S., Couch, W. J., & Carter, D. 1993, *MNRAS*, 262, 764
- Barger, A. J., Aragon-Salamanca, A., Ellis, R. S., Couch, W. J., Smail, I., & Sharples, R. M. 1996, *MNRAS*, 279, 1
- Beers, T. C., Flynn, K., & Gebhardt, K. 1990, *AJ*, 100, 32
- Bender, R., Saglia, R. P., Ziegler, B., Belloni, P., Greggio, L., & Hopp, U. 1997, *ApJ*, in press, astro-ph/9708237
- Biretta, J., Ritchie, C., & Rudloff, K. 1995, *STScI Science Report 95-06, A Field Guide to WFPC2 Image Anomalies*
- Bothun, G. D., & Gregg, M. D. 1990, *ApJ*, 350, 73
- Bower, R. G., Lucey, J. R., & Ellis, R. S. 1992a, *MNRAS*, 254, 589
- Bower, R. G., Lucey, J. R., & Ellis, R. S. 1992b, *MNRAS*, 254, 601
- Butcher, H., & Oemler, A. 1978, *ApJ*, 219, 18
- Butcher, H., & Oemler, A. 1984, *ApJ*, 285, 426
- Caldwell, N., Rose, J. A., Sharples, R. M., Ellis, R. S., & Bower, R. G. 1993, *AJ*, 106, 473
- Carlberg, R. G., Yee, H. K. C., & Ellingson, E. 1997, *ApJ*, 478, 462
- Couch, W. J., & Sharples, R. M. 1987, *MNRAS*, 229, 423
- Dressler, A. 1980, *ApJS*, 42, 565
- Dressler, A., & Gunn, J. E. 1983, *ApJ*, 270, 7
- Dressler, A., & Shectman, S. A. 1988, *AJ*, 95, 985
- Dressler, A., Oemler, A., Jr., Couch, W. J., Smail, I., Ellis, R. S., Barger, A., Butcher, H., Poggianti, B. M., & Sharples, R. M. 1997, *ApJ*, in press, astro-ph/9707232
- Ellis, R. S., Smail, I., Dressler, A., Couch, W. J., Oemler, A., Butcher, H., & Sharples, R. M. 1997, *ApJ*, 483, 582
- Evrard, A. E. 1990, *ApJ*, 363, 349
- Evrard, A. E. 1991, *MNRAS*, 248, p8
- Faber, S. M., Dressler, A., Davies, R. L., Burstein, D., Lynden-Bell, D., Terlevich, R., & Wegner, G. 1987, *Faber S. M., ed., Nearly Normal Galaxies*. Springer, New York, p. 175
- Fabricant, D. G., McClintock, J. E., & Bautz, M. W. 1991, *ApJ*, 381, 33
- Fisher, D., Fabricant, D., Franx, M., & van Dokkum, P. G. 1997, *ApJ*, in press
- Forman, W., Bechtold, J., Blair, W., Giacconi, R., van Speybroeck, L., & Jones, C. 1981, *ApJ*, 243, L133
- Franx, M., Illingworth, G., & Heckman, T. 1989, *AJ*, 98, 538
- Frenk, C. S., Evrard, A. E., White, S. D. M., & Summers, F. J. 1996, *ApJ*, 472, 460
- Geller, M. J., & Beers, T. C. 1982, *PASP*, 94, 421
- Godwin, J. G., Metcalfe, N., & Peach, J. V. 1983, *MNRAS*, 202, 113
- Gunn, J. E., & Gott, J. R. 1972, *ApJ*, 176, 1
- Guzman, R., Lucey, J. R., Carter, D., & Terlevich, R. J. 1992, *MNRAS*, 257, 187
- Hernquist, L., & Mihos, J. C. 1995, *ApJ*, 448, 41
- Holtzman, J. A., Burrows, C. J., Casertano, S., Hester, J. J., Trauger, J. T., Watson, A. M., & Worthey, G. 1995, *PASP*, 107, 1065
- Högbom, J. A. 1974, *A&AS*, 15, 417
- Jørgensen, I., Franx, M., & Kjærgaard, P. 1993, *ApJ*, 411, 34
- Jørgensen, I., & Franx, M. 1994, *ApJ*, 433, 553
- Kauffmann, G. 1995, *MNRAS*, 274, 153
- Kelson, D. D., van Dokkum, P. G., Franx, M., Illingworth, G. D., & Fabricant, D. 1997, *ApJ*, 478, L13
- Krist, J. 1995, in *Astronomical Data Analysis Software and Systems IV*, ASP Conference Series, 77, R. A. Shaw, H. E. Payne, and J. J. E. Hayes, eds., p. 349
- Lacey, C., & Cole, S. 1993, *MNRAS*, 262, 627
- Larson, R. B., Tinsley, B. M., & Caldwell, C. N. 1980, *ApJ*, 237, 692
- Lavery, R. J., & Henry, J. P. 1994, *ApJ*, 426, 524
- Leitherer 1995, ed., *HST Data Handbook Version 2.0*, STScI, Baltimore
- Luppino, G. A., Cooke, B. A., McHardy, I. M., & Ricker, G. R. 1991, *AJ*, 102, 1
- Mazure, A., Proust, D., Mathez, G., & Mellier, Y. 1988, *A&AS*, 76, 339
- Moore, B., Katz, N., Lake, G., Dressler, A., & Oemler, A., Jr. 1996, *Nature*, 379, 613
- Pence, W. 1976, *ApJ*, 203, 39
- Pickles, A. J., & van der Kruit, P. C. 1991, *A&AS*, 91, 1
- Poggianti, B. M., & Barbaro, G. 1996, *A&A*, 314, 379
- Rakos, K. D., & Schombert, J. M. 1995, *ApJ*, 439, 47
- Rix, H.-W., & White, S. D. M. 1990, *ApJ*, 362, 52
- Saglia, R. P., Bertschinger, E., Baggley, G., Burstein, D., Colless, M., Davies, R. L., McMahan, R. K., Jr., & Wegner, G. 1997, *ApJS*, 109, 79
- Sandage, A., & Visvanathan, N. 1978, *ApJ*, 225, 742
- Sérsic, J. L. 1968, *Atlas de galaxias australes*, Observatorio Astronómico de Córdoba, Argentina
- Smail, I., Dressler, A., Couch, W. J., Ellis, R. S., Oemler, A., Jr., Butcher, H., & Sharples, R. M. 1997, *ApJS*, 110, 213
- Stanford, S. A., Eisenhardt, P. R., & Dickinson, M. 1997, *ApJ*, in press, astro-ph/9708037
- Thompson, L. A. 1986, *ApJ*, 306, 384
- Tinsley, B. M. 1980, *Fundam. Cosmic Phys.*, 5, 287
- van Dokkum, P. G., & Franx, M. 1996, *MNRAS*, 281, 985
- White, S. D. M., Briel, U. G., & Henry, J. P. 1993, *MNRAS*, 261, L8
- Whitmore, B. 1997, *Photometry with the WFPC2*, STScI, Baltimore
- Worthey, G. 1994, *ApJS*, 95, 107

TABLE 1  
GALAXY CATALOG

| Id | $x$ (") | $y$ (") | type | $n$ | $F814W$ | $V_z$ | $F606W - F814W$ | $(B-V)_z$ | $r_c$ (") |
|----|---------|---------|------|-----|---------|-------|-----------------|-----------|-----------|
| 86 | -60.9   | -252.6  | E    | 1   | 20.78   | 21.68 | 1.179           | 0.837     | 0.32      |
| 92 | 137.2   | -237.1  | S0   | 2   | 19.84   | 20.75 | 1.201           | 0.855     | 0.60      |
| 95 | 63.5    | -235.4  | E    | 3   | 19.32   | 20.25 | 1.249           | 0.894     | 0.52      |

NOTE.—Table 1 is published in its entirety in the AAS CD-ROM Series.

TABLE 2  
OFFSET AND SCATTER OF THE CM RELATION

| Sample          | $N$ | Offset | Error | Obs. Scatter | Intr. Scatter | Error |
|-----------------|-----|--------|-------|--------------|---------------|-------|
| All             | 188 | -0.012 | 0.003 | 0.041        | 0.040         | 0.006 |
| E               | 46  | 0.000  | 0.003 | 0.024        | 0.022         | 0.003 |
| S0              | 95  | -0.012 | 0.003 | 0.031        | 0.029         | 0.004 |
| S               | 7   | -0.141 | 0.032 | 0.092        | 0.091         | 0.051 |
| Irr             | 9   | -0.292 | 0.027 | 0.086        | 0.085         | 0.023 |
| $n = 4$         | 46  | -0.008 | 0.003 | 0.024        | 0.022         | 0.005 |
| $n = 3$         | 80  | -0.011 | 0.004 | 0.036        | 0.034         | 0.006 |
| $n = 2$         | 32  | -0.022 | 0.010 | 0.061        | 0.060         | 0.026 |
| $n = 1$         | 30  | -0.117 | 0.026 | 0.154        | 0.154         | 0.021 |
| $E < 118''$     | 24  | 0.003  | 0.005 | 0.024        | 0.021         | 0.004 |
| $E \geq 118''$  | 22  | -0.003 | 0.005 | 0.025        | 0.023         | 0.006 |
| $S0 < 118''$    | 46  | -0.005 | 0.003 | 0.021        | 0.018         | 0.004 |
| $S0 \geq 118''$ | 49  | -0.019 | 0.006 | 0.043        | 0.041         | 0.009 |

Fig. 1.— *Hubble Space Telescope* WFPC2 mosaic of the cluster CL 1358+62 at  $z = 0.33$ . The image is a mosaic of twelve adjacent HST pointings, in two filters ( $F606W$  and  $F814W$ ). The  $F606W$  and  $F814W$  images were added to increase the S/N, giving a total exposure time of 7200 s per pointing (3600 s in each filter). North is up and East is to the left. The length of the scalebar is 1 arcmin, or  $350 h_{50}^{-1}$  kpc at the distance of CL 1358+62 ( $q_0 = 0.5$ ). The total area of the image is  $49 \text{ arcmin}^2$ . The galaxy density decreases with distance from the cluster center and BCG. The galaxy population in this intermediate  $z$  cluster can be studied in lower density regions than in previous studies with HST, which focussed on the cluster cores.

Fig. 2.— Color representation of the central part of Fig. 1 [Plate 1], created from the  $F606W$  and  $F814W$  exposures. The cluster members are easily recognized by their yellow colors. However, many of the bluer galaxies are also cluster members.

Fig. 3.— Greyscale representations of all spectroscopically confirmed cluster members in the CL 1358+62 HST mosaic. The boxes are  $6''4$ , or  $37 h_{50}^{-1}$  kpc ( $q_0 = 0.5$ ), on a side.

Fig. 4.— Examples of early-type galaxies on the CM relation, examples of slightly blue early-types, all very blue early-types, all spirals, and examples of irregular galaxies. Each box is  $6''4 \times 6''4$  ( $37 \times 37 h_{50}^{-1}$  kpc). The number in the lower right of each box is the galaxy identification, the number in the lower left is the restframe  $B-V$  color with respect to the CM relation. The slightly blue early-type galaxies have very similar morphologies to the early-types on the CM relation. The very blue early-types have low luminosities and generally have significant disks.